THERMAL EFFECTS ON THE DIESEL INJECTOR PERFORMANCE THROUGH ADIABATIC 1D MODELLING. PART II: MODEL VALIDATION, RESULTS OF THE SIMULATIONS AND DISCUSSION

Payri, R., Salvador, F.J., Carreres, M. (*), Belmar-Gil, M.

CMT-Motores Térmicos, Universitat Politècnica de València

Camino de Vera s/n, E-46022 Spain

(*) Corresponding author:

Dr. Marcos Carreres, marcarta@mot.upv.es

CMT-Motores Térmicos, Universitat Politècnica de València

Camino de Vera s/n, E-46022 Spain

Telephone: +34-963876540

Fax: +34-963877659

ABSTRACT

In this paper, a one-dimensional computational model of the flow in a common-rail injector is used to compute local variations of fuel temperature (including the temperature change produced upon expansion across the nozzle) and analyse their effect on injector dynamics. These variations are accounted through the adiabatic flow hypothesis, assessed in a first part of the paper where the model features are also described. They imply variations in the fuel properties and the flow regime established across the injector internal restrictions driving the solenoid valve. An extensive validation of the model against experimental results is presented for a wide range of conditions. Multiple injection strategies are also explored, analysing the influence of the inlet fuel temperature and its variations on the mass injected by successive injections and the critical dwell time below which they cannot be separated. Results show significant changes in fuel temperature across some injector restrictions. These changes are greater the highest the rail pressure and lowest the fuel temperature at the injector inlet. In the case of the flow across nozzle orifices, the fuel can be either heated or subcooled depending on the operating conditions, the heating being especially relevant for cold-start-like fuel temperatures at the inlet. Thermal effects also influence the injection rate and duration. This influence on injector dynamics is particularly accused in the injector of study due to its ballistic nature. In this regard, the time needed to effectively separate two successive injections is greater the higher the fuel temperature and the injection pressure.

Payri, R., Salvador, F.J., Carreres, M., Belmar-Gil, M., "Thermal effects on the diesel injector performance through adiabatic 1D modelling. Part II: Model validation, results of the simulations and discussion", Fuel 260:115663 (author version).

doi: 10.1016/j.fuel.2019.115663

KEYWORDS

diesel, injection, computational, 1D modelling, fuel temperature, adiabatic flow

LIST OF NOTATION

A_o outlet area

Ad adiabatic number

C_a area coefficient

C_d discharge coefficient

CN cavitation number

D diameter

D_{cl} clearance on diameter

D_{pist} piston diameter

D_0 orifice outlet diameter

F_{fric} force due to friction

F_{needle} force acting on the needle

$F_{\Delta p}$ force due to pressure differences

h specific enthalpy

L length

L_{cl} clearance length

l needle lift

m_i total mass injected per cycle

$\dot{m}_f$ fuel mass flow

Nu Nusselt number

Pr Prandtl number

p pressure

p_{cv} pressure in the control volume

p_{dw} downstream pressure

p_i injection pressure

p_{up} upstream pressure

p_v vapour saturation pressure

Payri, R., Salvador, F.J., Carreres, M., Belmar-Gil, M., “Thermal effects on the diesel injector performance through adiabatic 1D modelling. Part II: Model validation, results of the simulations and discussion”, Fuel 260:115663 (author version).

doi: 10.1016/j.fuel.2019.115663

Re Reynolds number
T temperature
T_{dw} downstream temperature
T_i fuel temperature at the injector inlet
T_{up} upstream temperature
T_w wall temperature
t time
t_{aSOE} time after the injector Start of Energizing
U_n needle velocity
u flow velocity

GREEK SYMBOLS

ρ_f fuel density
μ_f fuel dynamic viscosity

ABBREVIATIONS

DT Dwell Time
ET Energizing Time
NFL nozzle feeding line
OA control volume outlet orifice
OZ control volume inlet orifice
ROI Rate of Injection

1. INTRODUCTION

Great effort has traditionally been placed on the research and development of the fuel injection system, due to its role on the air-fuel mixture, combustion and formation of emissions [1–3]. The current scenario involving an ever growing population and an increase in their transportation needs, together with the limited availability of fossil fuels [4,5], lead to raised concerns and environmental awareness culminating in strict regulations in the matter such as the Euro 6 in Europe and those yet to come. Technological responses to comply with these regulations, such as the gradual increase in injection pressure [6,7] or the use of split injection strategies [8–11], have resulted in a greater complexity of the injection system. This fact highlights the need for computational tools that allow to predict and understand its behaviour for a wide range

Payri, R., Salvador, F.J., Carreres, M., Belmar-Gil, M., “Thermal effects on the diesel injector performance through adiabatic 1D modelling. Part II: Model validation, results of the simulations and discussion”, Fuel 260:115663 (author version).

doi: 10.1016/j.fuel.2019.115663

of realizable conditions.

In this sense, 1D modelling appears to be an appropriate solution, since it may provide a deep insight on the complete injection process at a low computational cost compared to computationally expensive 3D CFD simulations usually restricted to a specific part of the injector [12–14] or to spray development [15]. In fact, the 1D modelling approach has been used by the authors in the past in order to study the injection system behaviour [16–18].

Temperature and pressure significantly modify the fuel properties that are relevant in the injection process (namely density, viscosity and speed of sound) [19]. Several researchers have experimentally studied the influence of the fuel temperature and the associated fuel properties on the spray formation [20,21], but generally left injector dynamics out of their scope. Wang et al. [22] did study the effect of the fuel temperature on the performance of split injection strategies, finding that cold conditions reduced the interaction among split injection events. With the aid of 1D modelling, the authors of the present investigation tried to start the study upstream of the nozzle in order to further understand the mechanisms behind the experimental findings, despite treating the flow as isothermal [17]. We found the flow regime induced by the operating conditions (including the fuel temperature at the injector inlet) on the nozzle and the control volume orifices could importantly drive needle dynamics. However, the model capabilities did not allow the study of the effect of split injections. The purpose of this work is to gain further understanding on the topic thanks to the use of a 1D model improved by the implementation of the adiabatic flow assumption. Details on the implementation of this hypothesis and the assessment of its validity for realistic conditions are addressed in the first part of the paper [23]. In the current paper, the model is extensively validated against experimental results and then used to quantitatively estimate the fuel temperature variations along a solenoid-driven common-rail injector. This prediction allows to study the influence of the fuel temperature and its changes on injector dynamics and the injection rate shape thanks to the analysis of the flow regime that these variations establish on the internal orifices driving the solenoid valve. On the other hand, the estimation of the fuel temperature at the injector outlet will be relevant for experimentalists in the field and CFD modellers in need of suitable boundary conditions. Additionally, since the propagation of the pressure wave along the injector will have been validated, split injection strategies are also explored. In this regard, the time needed to split successive injections is determined as a function of the inlet fuel temperature and the rail pressure. An assessment on the influence of these operating conditions on the mass injected by separated injections is also carried out.

2. VALIDATION OF THE 1D ADIABATIC MODEL OF THE INJECTOR

In the first part of the paper, the validity of the adiabatic flow hypothesis has been evaluated and it has been established that, prior to a given injection, it may be necessary to consider a certain fuel temperature change at the injector inlet with respect to the fuel temperature in the rail [23]. Keeping this fact in mind, the model of the Bosch CRI 2.20 implemented in AMESim (here reproduced as Figure **1** for illustrating purposes) can now be validated as a whole for a wide range of operating conditions. This validation is carried out in two steps. First, the ability of the model to estimate the mass flow rate and the temperature change across a single hydraulic restriction is tested under continuous flow. Once the proper behaviour is ensured for each orifice, the model capabilities in terms of predicting the way the pressure waves are transmitted along the injector (mandatory for a proper description of the multiple injection strategies) and the delivered ROI are ensured for regular pulsed injections.

Payri, R., Salvador, F.J., Carreres, M., Belmar-Gil, M., “Thermal effects on the diesel injector performance through adiabatic 1D modelling. Part II: Model validation, results of the simulations and discussion”, Fuel 260:115663 (author version).

doi: 10.1016/j.fuel.2019.115663

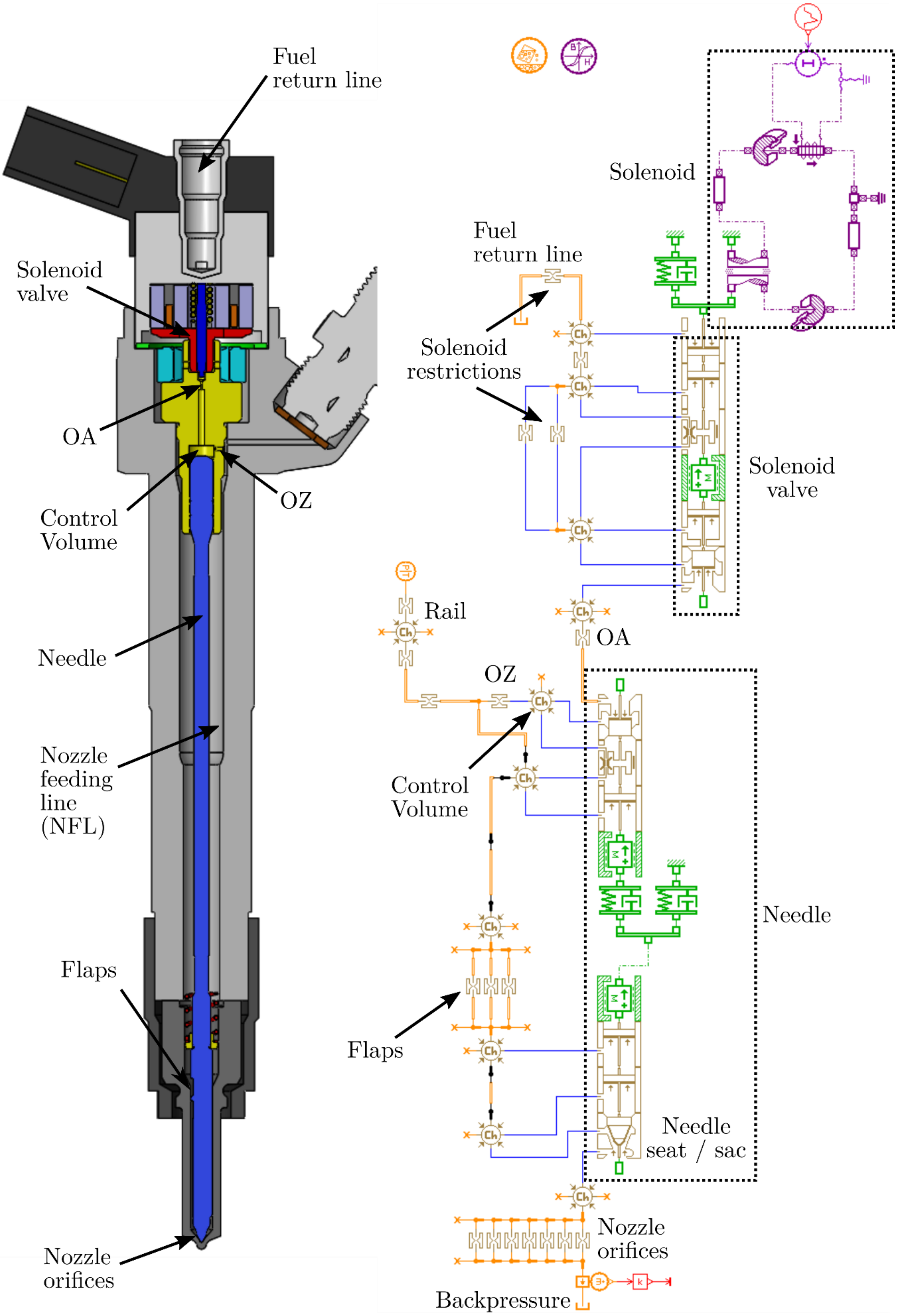

124

125 Figure 1. Bosch CRI 2.20 injector diagram and AMESim model sketch.

2.1. Mass flow rate prediction through a single injector orifice

Prior to the validation of the injector as a whole, the behaviour of the most significant hydraulic restrictions of the injector (namely the OZ, OA and nozzle orifices; seen in **Figure 1**) was independently validated against experimental measurements of mass flow rate under continuous flow carried out by the authors in a previous work [24]. As stated in the first part of the paper [23], these measurements were taken by isolating the orifice to be tested within a purpose-built test rig and submitting it to a controlled pressure drop. Specifically, this was achieved by setting a value of upstream pressure (p_{up}) and independently modifying the downstream pressure (p_{dw}). This procedure was repeated for several values of upstream pressure. Conditions tested to reproduce all the possible flow regimes induced during the regular operation of the injector are compiled in Table **1**. In the particular case of the multi-hole nozzle, the large effective area of the 7 orifices prevented the two largest values of p_{up} from being tested, due to flow rate limitations in the high pressure pump.

p_{up} [MPa]	p_{dw} [MPa]
5	0.5, 1, 1.5, 2, 2.5, 3, 3.5, 4, 4.2, 4.4, 4.6, 4.8
10	0.5, 1, 1.5, 2, 2.5, 3, 4, 5, 6, 7, 8, 9
20, 30, 40, 50, 60	0.5, 1, 1.5, 2, 2.5, 3, 4, 5, 6, 7, 8, 9, 10, 11, 12

Table 1. Conditions considered in the independent validation of the flow through the injector internal orifices.

The experimental facility was reproduced in AMESim with the same model of the orifice used for the complete injector model. Results of this validation are shown in **Figure 2**. Focusing on the nozzle orifices, **Figure 2(a)** shows that the mass flow rate is linear with respect to the square root of the pressure drop. This implies that the nozzle does not cavitate for any of the operating conditions tested [25,26]. Results show a good agreement for most of the pressure conditions tested. The highest deviations in the predictions take place for the lowest values of the pressure drop, resulting in an underestimation of the mass flow rate. The explanation for these deviations resides in the low values of *Re* established for these conditions, which induce a laminar flow regime or the laminar-turbulent transitional regime. In these flow regimes, the nozzle orifices discharge coefficient has not reached its asymptotic behaviour yet [27]. The model computes the discharge coefficient at each time step through a certain function of the local *Re*, as described in the previous work by the authors on the isothermal variant of the model [17]. This modelled trend could lead to larger deviations in the regime transition. Anyway, the deviations are bounded for values of $\Delta p^{1/2} > 3$ (i.e. pressure drops around 9 MPa), reached in the injector nozzle for the typical engine operating conditions).

Payri, R., Salvador, F.J., Carreres, M., Belmar-Gil, M., “Thermal effects on the diesel injector performance through adiabatic 1D modelling. Part II: Model validation, results of the simulations and discussion”, Fuel 260:115663 (author version).

doi: 10.1016/j.fuel.2019.115663

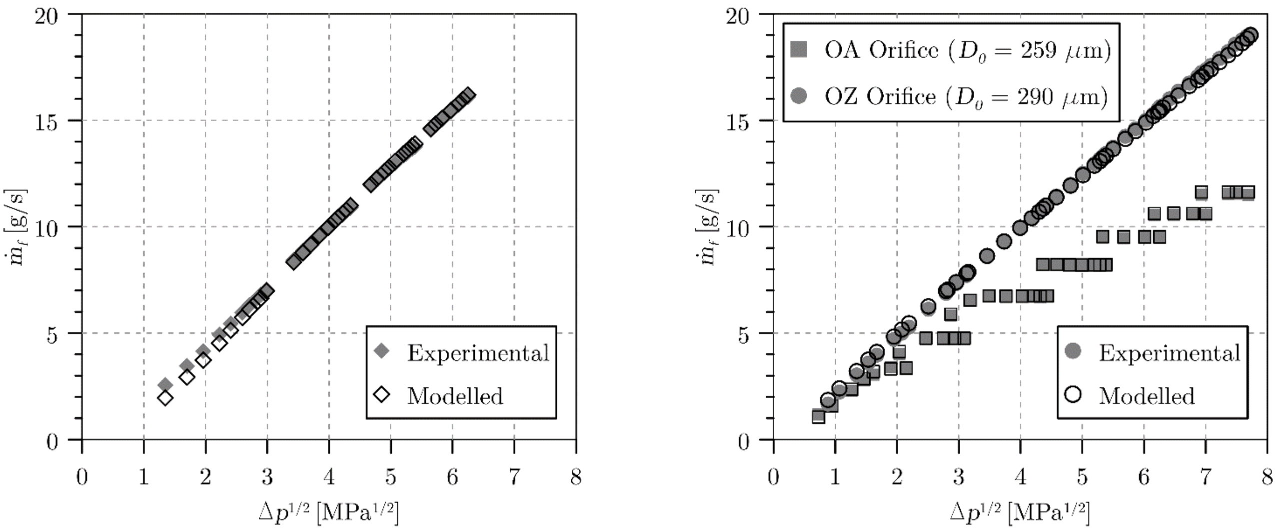

(a) Nozzle orifices (7 orifices with $D_o = 117 \pm 1\ \mu$m). (b) Control volume orifices.

Figure 2. Modelled mass flow rate through the injector internal orifices compared against experimental data.

The comparison for the control volume orifices is shown in **Figure 2(b)**. In the case of the OZ orifice, cavitation is not found either and the mass flow rate predictions show a good agreement with the experimental measurements. Focusing on the OA orifice, a mass flow collapse is detected for each value of upstream pressure from a certain value of downstream pressure. The deviations among the predictions and the experiments are negligible, also demonstrating the ability of the model to predict the appearance of cavitation.

2.2. Temperature change prediction through a single injector orifice

As stated in the first part of the paper [23], the temperature changes across an injector restriction are computed considering the adiabatic flow assumption through Eq. (1):

$$h(T_{dw}, p_{dw}) = h(T_{up}, p_{up}) - \frac{1}{2}\Delta u^2 \tag{1}$$

For the restrictions where the velocity change is not relevant (such as the nozzle feeding line), Eq. (1) leads to the conservation of specific enthalpy in order to calculate the temperature changes through them. In the particular orifices submitted to large pressure drops (such as the nozzle orifices and the OA orifice), Eq. (1) could be approximated by Eq. (2):

$$h(T_{dw}, p_{dw}) \approx h(T_{up}, p_{up}) - \left(\frac{C_d}{C_a}\right)^2 \frac{(p_{up} - p_{dw})}{\rho_f} \tag{2}$$

It is important to note here that cavitation leads to a local cooling associated with the enthalpy of phase change. This phenomenon is not taken into account by the model, considering its relatively low importance as found by Franc [28] for

doi: 10.1016/j.fuel.2019.115663

other fluids and checked by the authors in the case of diesel fuel (in the order of 10^{-3} K). In addition, as highlighted in **Section 2.1**, cavitation was only found in the OA orifice. Therefore, the omission of the enthalpy phase change due to cavitation is not expected to influence the validity of the model estimations.

In this Section, the temperature changes predicted by the model across the OZ orifice (for which $C_a = 1$ due to the absence of cavitation [29]) are compared to experimental results. In the experiments used as a basis for the validation of Section 2.1, the temperature variation across the injector internal orifices was also measured for the set of upstream and downstream conditions depicted in Table **1** [24], controlling the upstream temperature at all times so that $T_{up} = 293$ K.

Figure **3** shows the results of the comparison of the temperature drop predicted by the model against the experimental results for the OZ orifice. As expected according to the *specific enthalpy map* of the winter diesel fuel presented in the first part of the paper [23], the temperature change upon expansion tends to increase linearly with the pressure drop. The computational results offer a good prediction of the experimental data, with the higher deviations being present for the lowest values of pressure drop. This fact is aligned with the findings of the previous work by the authors [24], in which the dimensionless parameter defined in Eq. (3) was derived to establish the variables that influenced the proneness of the flow through an orifice to exchange heat with the surroundings.

$$Ad = \frac{1}{4}\frac{D}{L}St^{-1} = \frac{1}{4}\frac{D}{L}\frac{Pr\ Re}{Nu} \tag{3}$$

The different diameter of the internal orifices and the different conditions (i.e. pressure drops) experimentally tested were associated to several values of *Ad*. It was found that low values of *Ad* ($Ad < 4$) could lead to a significant heat exchange during the process, whereas high values of *Ad* ($Ad > 6$) led to heat transfer being practically negligible. Thus, the lowest pressure drops in Figure **3** lead to low values of *Ad* for which heat transfer from the surroundings prevents the adiabatic flow assumption from being accurate. Nevertheless, such low values of pressure drop only take place during short transients at the injector opening (when the pressure at the control volume is still close to the rail pressure) or closing, but they do not take place across this orifice during the steady operation of the injector. Please note that the heating produced inside the OZ orifice for a pressure drop of 60 MPa (representative of the steady pressure drops established through this orifice for usual engine operating conditions) is close to 30 K. This increase can affect the fuel properties at the orifice outlet, influencing injector dynamics, as explored in the present investigation.

doi: 10.1016/j.fuel.2019.115663

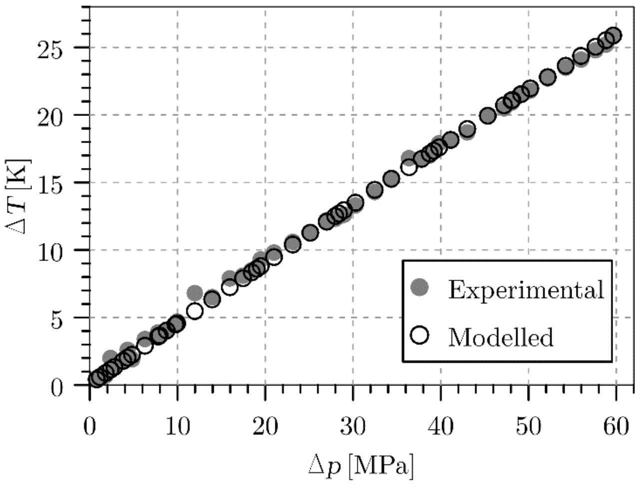

Figure 3. Modelled temperature change through the injector OZ orifice compared against experimental data.

2.3. Pressure waves transmission

Once the injector computational model has been partially validated by ensuring its ability to predict the individual behaviour of the internal orifices, the accuracy of the predictions of the complete injector model must be tested for a wide range of operating conditions. As the first step to this end, the modelled evolution of the pressure at the injector inlet is compared to the experimental evolution found at this location for the ROI measurements performed in a previous work [30]. This comparison allows to assess the capability of the model to describe the propagation of the pressure wave along the injector. This capability is key to ensure a proper prediction of the injector behaviour under split injection strategies, considering that once an injection finishes, the induced pressure wave influences the next injection event depending on the timing among injections.

The operating conditions for which the ROI measurements were taken are summarized in Table **2**. A wide range of values of the fuel temperature at the injector inlet (from those ones representative of cold-start to those others representative of long engine runs), injection pressures and energizing times (from short injections to injections long enough to ensure that the steady conditions are accurately described) are considered. It is important to note that these experimental measurements were taken in a laboratory environment in which T_i was controlled and the hardware was thermally insulated so that $T_i = T_w$. This implies that the heat transfer process in the time lapse among injections is not relevant. Heat transfer could only take place during the injection itself if the *Ad* values induced across the injector hydraulic restrictions were low. It was already stated in Section 2.2 that this might be the case during the transient stages (injector opening and closing), whereas in steady-state conditions it can be ensured that *Ad* is high enough to prevent heat transfer from being relevant. In short, heat transfer in the experiments could only be relevant to some extent during the transient stages of the injection, being negligible when steady-state conditions are reached. In these conditions, the flow can be

doi: 10.1016/j.fuel.2019.115663

safely regarded to as adiabatic.

Property	Values tested
T_i [K]	253 – 273 – 303 – 353 – 373
p_i [MPa]	40 – 70 – 120 – 180
p_b [MPa]	4
ET [ms]	0.25 – 0.5 – 1

Table 2. Operating conditions tested in the experimental ROI measurements used to validate the injector model.

Sample comparisons among the modelled and the experimental pressure evolution at the high-pressure line connecting the *common-rail* to the injector are shown in Figure **4**, covering the conditions corresponding to the most extreme values of speed of sound in the ROI measurements (low pressures and high temperatures on the one hand, with high pressures and low temperatures on the other). Different energizing times are also shown. As can be seen, the model accurately represents the pressure evolution for most of the tested points. The first drop in pressure, which coincides with the injector opening, always takes place slightly later for the injector model. As highlighted by the points corresponding to ET = 0.5 ms, both the period and the amplitude of the oscillations are properly predicted. The amplitude of the second pressure peak is underestimated, although the differences seem to be reduced for the next peak. Results for the extreme energizing times are less accurate, especially in terms of amplitude, even though the period of the oscillations seems to be captured. The proper matching of this last parameter is essential for the model behaviour, since it defines the trends followed by the mass injected by post-injections depending on the dwell time among injections, as explored in Section 4.

doi: 10.1016/j.fuel.2019.115663

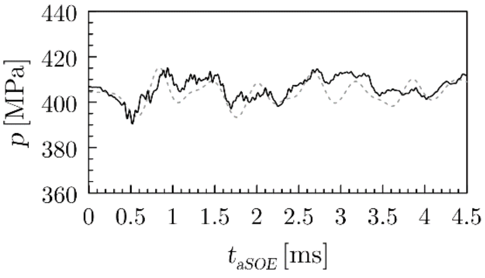

(a) $p_i = 40$ MPa, $T_i = 373$ K, ET = 0.25 ms

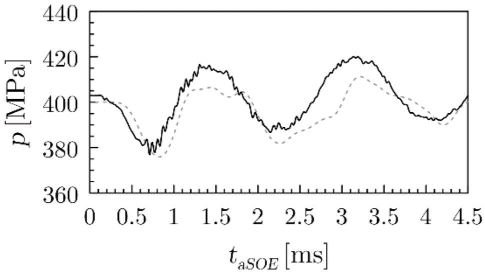

(b) $p_i = 40$ MPa, $T_i = 373$ K, ET = 0.5 ms

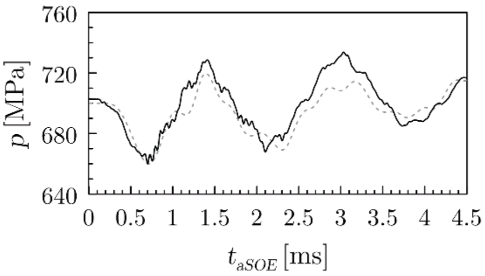

(c) $p_i = 70$ MPa, $T_i = 353$ K, ET = 0.5 ms

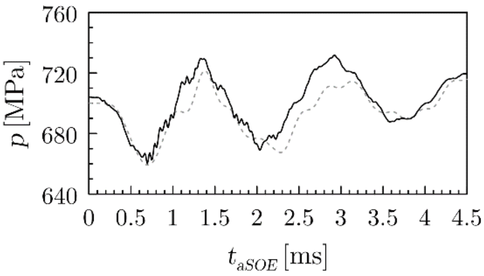

(d) $p_i = 70$ MPa, $T_i = 303$ K, ET = 0.5 ms

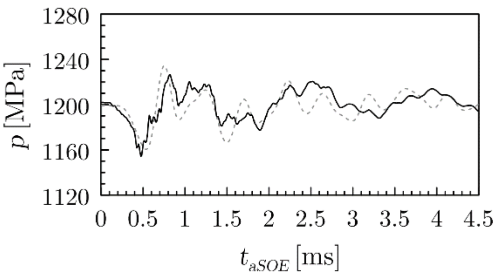

(e) $p_i = 120$ MPa, $T_i = 303$ K, ET = 0.25 ms

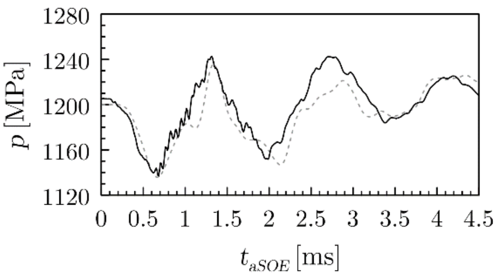

(f) $p_i = 120$ MPa, $T_i = 303$ K, ET = 0.5 ms

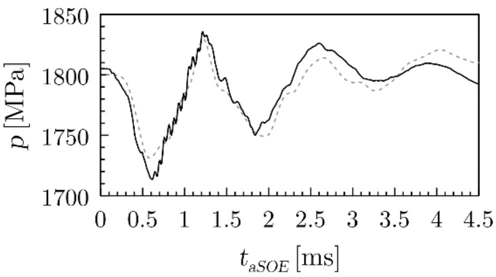

(g) $p_i = 180$ MPa, $T_i = 253$ K, ET = 0.5 ms

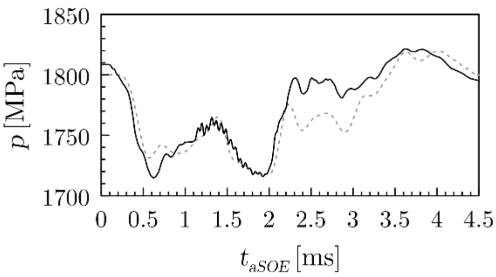

(h) $p_i = 180$ MPa, $T_i = 253$ K, ET = 1 ms

Figure 4. Modelled pressure signal (dashed) at the common-rail high pressure line compared against experimental data (continuous).

2.4. Prediction of the mass flow rate at the injector outlet

The analysis of the behaviour in terms of fuel delivery by the injector is the last step to validate the computational model.

Figure **5** shows the comparison of the modelled ROI with the experimental data for the extreme values of fuel temperature

doi: 10.1016/j.fuel.2019.115663

at the injector inlet for the different energizing times tested. These experimental data are available in a previous work by the authors [30], where details on the experimental campaign and the methodology employed to control the fuel temperature at the injector inlet were reported. Further details on the processing, filtering and correction of the measured signal in order to obtain ROI curves with the Bosch long tube method can also be found in a previous work by the authors [31]. The authors quantified the uncertainty of this methodology in providing the injected mass flow rate to be lower than 2%.

On the one hand, Figure **5** reproduces the main findings previously reported in [30] concerning injector dynamics and the steady-state stage of the injection: the injector opening is slower for low values of T_i, due to the high fuel viscosities associated to low temperatures. This fact delays needle dynamics due to an enhancement of viscous friction and a change in the flow regime in the control volume orifices, as will be quantified in Section 4. This effect is more accused for low injection pressures. In addition, the injection duration is appreciably reduced the lower the value of fuel temperature. This can be explained due to the ballistic nature of the injector, considering that the increase in viscosity at low temperatures results in a lower position of the needle being achieved during the injector energizing. Therefore, the distance the needle needs to travel to close back against its seat is shorter, travelling it in reduced times. As far as the steady-state stage of the injection is concerned, the experimental results depicted in Figure **5** were analysed in the previous work, showing that for low injection pressures the steady-state ROI increases when the fuel temperature increases (despite the reduction in fuel density), whereas for high injection pressures the steady-state ROI decreases when the fuel temperature increases. This was explained considering the opposed effects of the fuel temperature on the mass flow rate through the fuel density itself and through the discharge coefficient (in turn influenced by the fuel density and viscosity). In any case, the relative differences among cases are found to be low, and they could already be satisfactorily explained without the aid of the model. They are thus not analysed in the present work since the local variations of fuel temperature do not give a deeper insight into the topic.

On the other hand, Figure **5** proves the ability of the adiabatic model to predict the actual behaviour of the injector, both during the transient and steady stages of the injection event. The predictions are reasonable for most operating conditions, with a certain underprediction of the mass flow rate during the opening for the extreme case of low pressure and low temperature. Precisely, these are the conditions for which the adiabatic flow assumption is less valid, due to the low values of *Re* induced to the flow through the orifices, resulting in turn in a low *Ad* even during the steady-state stage of the injection. Nevertheless, it must be noted that the previous version of the model presented by the authors (using the assumption of isothermal flow) could not be validated for $T_i < 273$ K [17]. It can then be stated that the introduction of the assumption of adiabatic flow allows widening the range of injector operating conditions for which a 1D model is valid, including the extreme temperature conditions found for the cold-start operation of the injector.

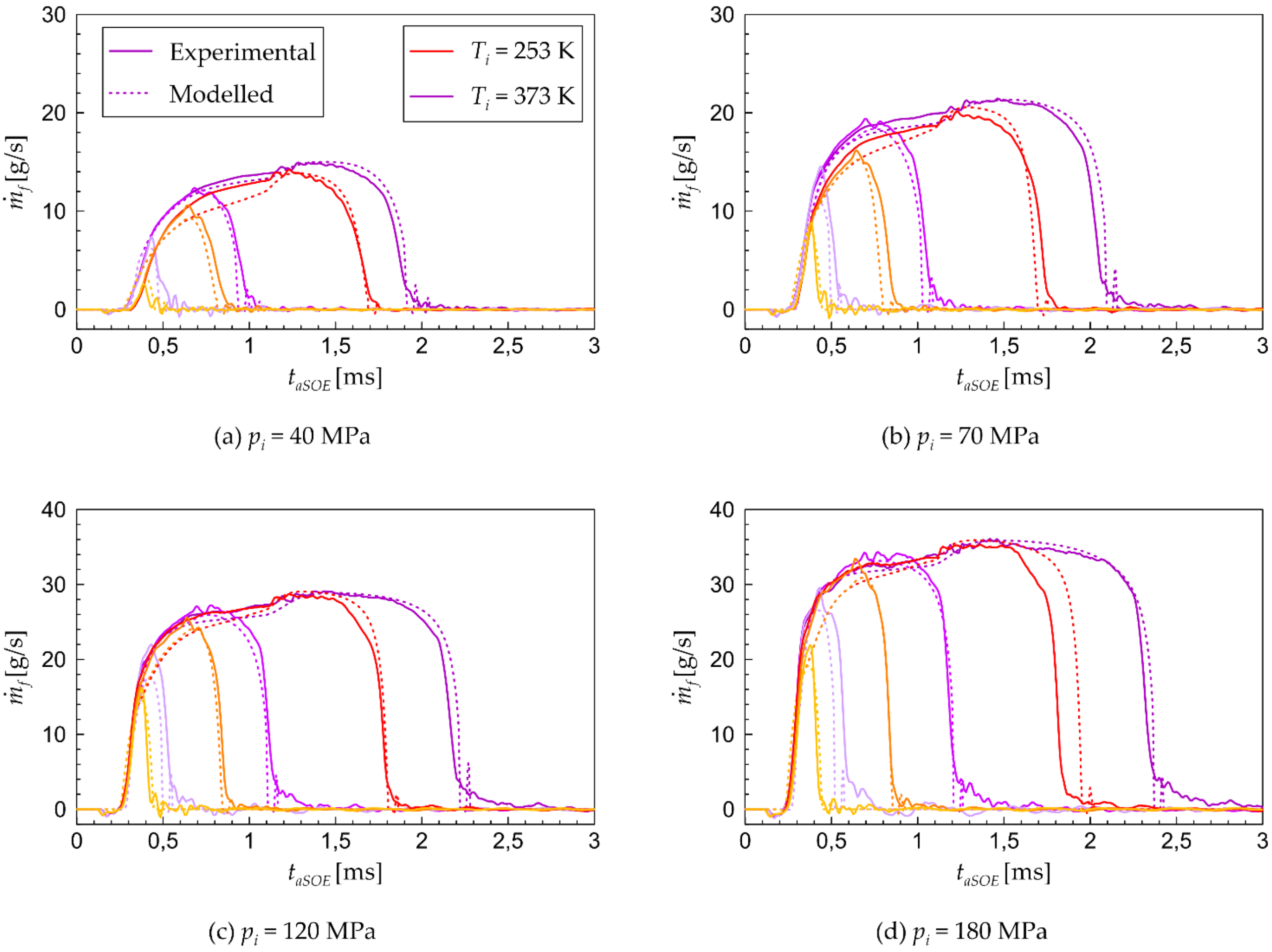

Figure 5. Modelled ROI compared against experimental data from [30]. Each plot shows results for ET = 0.25 ms (light color), ET = 0.5 ms (medium color) and ET = 1 ms (dark color).

As a summary of the validation results, including all the operating conditions compiled in Table **2**, **Figure 6** shows the comparison between the modelled and experimental results of total mass injected per injection event. The lines representing the perfect matching and 5% of deviation are also depicted. Results show a fair prediction for most of the operating conditions studied, as a consequence of the findings from Figure **2** to Figure **5**. More than 90% of the conditions leading to m_i > 10 mg/st show deviations lower than 5%. The conditions resulting in the poorest predictions generally correspond to the extreme cases of injection pressure and temperature. The injections corresponding to m_i < 8 mg/st are shown in Figure **6(b)**. For those conditions, more than 70% of the tested points have been predicted with a deviation lower than 25%. It should be noted that, for these small quantities, short absolute deviations lead to a high percentage of deviation even if the ROI curve is accurately modelled.

doi: 10.1016/j.fuel.2019.115663

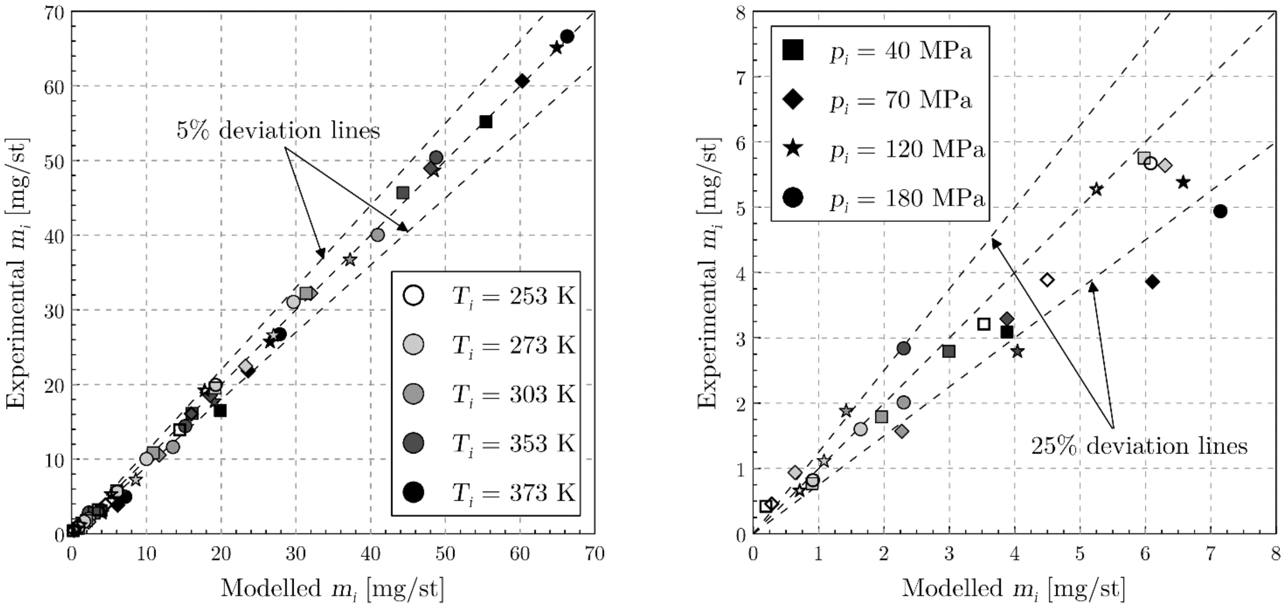

(a) All operating conditions tested. (b) Detail of the short injections.

Figure 6. Modelled mass injected per stroke compared against experimental data.

3. MODEL PREDICTION OF THE FUEL TEMPERATURE VARIATIONS ALONG THE INJECTOR

The temperature variations computed by the model through the most important injector restrictions during a pulsed injection are analysed in this Section. These temperature changes result in variations in the fuel properties that, in turn, establish the flow regime across the restrictions controlling injector dynamics. Hence, the resulting flow regime in the orifices is identified for each injector operating condition, allowing to determine the conditions for which the pressure in the control volume drops in a quicker way. This evolution of the pressure in the control volume, together with the viscous forces opposing the needle motion, will help analysing injector dynamics in Section 4.

3.1. Analysis for the control volume orifices and hydraulic lines

Figure **7** shows the predicted temperature changes across the control volume orifices and the nozzle feeding hydraulic line NFL (line among the OZ orifice and the nozzle sac, recall Figure **1**), deemed to be the most important ones in the possible paths of the fuel along the injector. For each restriction, the temporal evolution of the temperature variation is presented for the different values of p_i tested and a sample value of T_i (ET = 1 ms). As a synthesis, the maximum temperature change registered for each operating condition is also shown for each restriction.

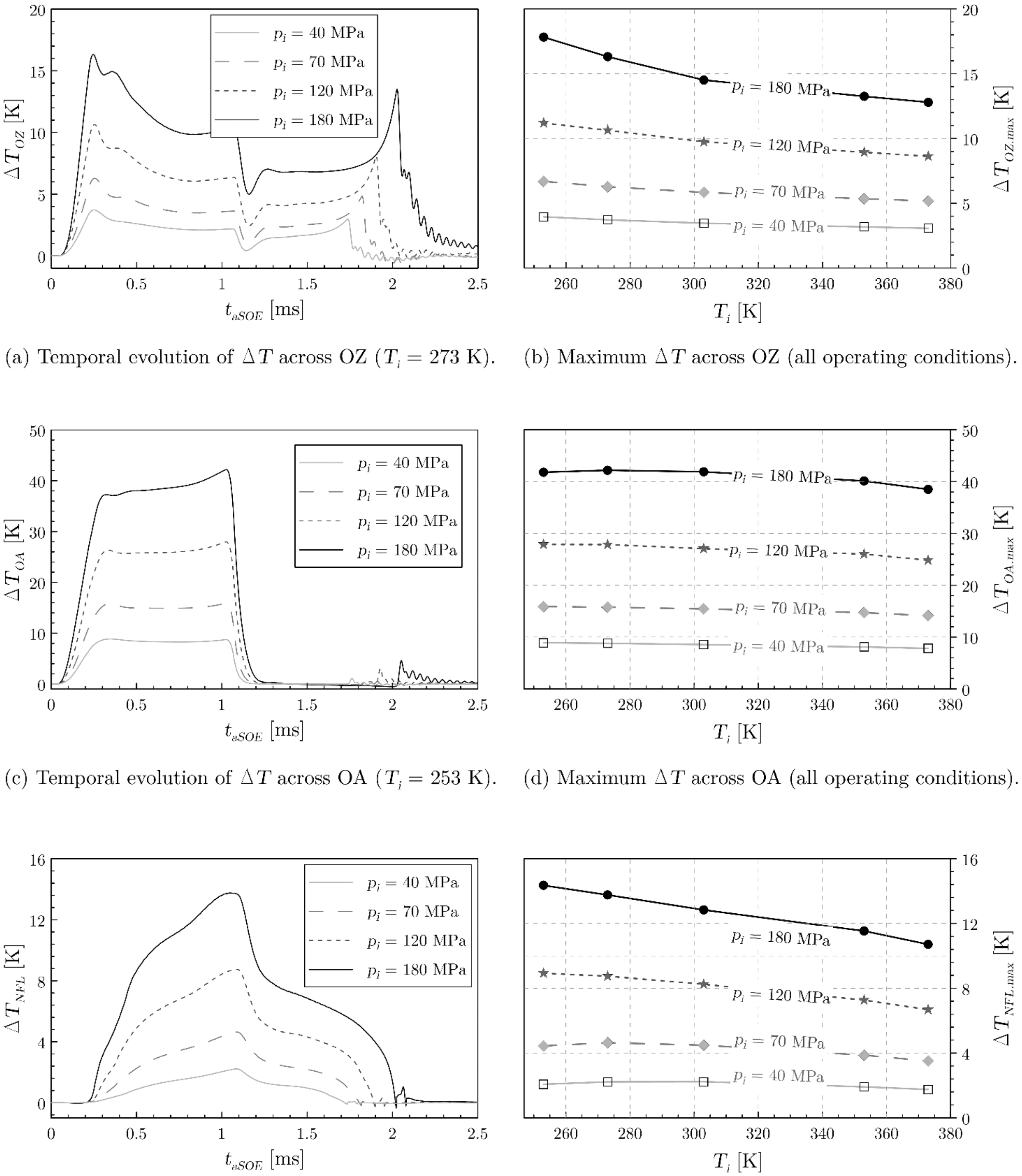

(a) Temporal evolution of ΔT across OZ ($T_i = 273$ K).

(b) Maximum ΔT across OZ (all operating conditions).

(c) Temporal evolution of ΔT across OA ($T_i = 253$ K).

(d) Maximum ΔT across OA (all operating conditions).

(e) Temporal evolution of ΔT along NFL ($T_i = 303$ K).

(f) Maximum ΔT along NFL (all operating conditions).

Figure 7. Temperature changes across the control volume orifices and the nozzle feeding line.

Starting with the OZ orifice, Figure **7(a)** shows that the fuel temperature increases through the orifice during the whole injection. Considering that this restriction generates a pressure drop in the control volume, this fact is consistent with the reasoning made in the first part of the paper [23] (in the view of Eq. (1) and considering a negligible velocity change across the orifice) about the fuel temperature increasing upon this adiabatic expansion. Therefore, the temperature rise is greater the higher the injection pressure, since the absolute pressure drop across the orifice also gets larger. The computed temperature change is not constant during the injection: after a first peak matching the injector opening stage ($t_{aSOE} \approx$ 0.3 ms), ΔT gets less important during the injection. This fact can be explained because the pressure upstream of the orifice decreases when a higher amount of fuel bypasses the OZ orifice inlet and leaves the injector through the nozzle feeding line and the nozzle orifices, resulting in a less important pressure drop through OZ. When the injector stops being energized and the pressure in the control volume is restored, the pressure drop across OZ is even lower, generating the valley in the curve ($t_{aSOE} \approx$ 1.2 ms). At this moment, the needle starts falling, leaving more room above it (i.e. in the control volume) for the fuel, which keeps being introduced through OZ. The orifice still generates a pressure drop that leads to the temperature rise observed until the injector completely closes.

Figure **7(a)** and Figure **7(b)** show that the maximum temperature change is greater the higher the injection pressure, as it has been justified. Moreover, for each injection pressure, the temperature increase is more accused the lower T_i. This fact can be attributed to the orifice working under a different flow regime at low temperatures. In this sense, Figure **8(a)** shows the modelled evolution of the discharge coefficient of the inlet orifice as a function of *Re*. As it may be seen, there is a certain temperature value from which no influence of T_i on the discharge coefficient is reported. Namely, for T_i > 303 K, the maximum discharge coefficient is already reached regardless of the injection pressure. On the contrary, for lower values of T_i, the higher fuel viscosity induces a laminar flow regime that leads to a lower discharge coefficient, implying higher losses through the orifice. As a consequence, the pressure drop established in the control volume is relatively larger than the one found for higher values of T_i, leading to a greater temperature rise across OZ as seen in Figure **7(b)**. This reasoning also explains why the trend of $\Delta T_{OZ,max}$ with T_i is not completely linear for the highest injection pressure, since the associated C_d importantly varies in this region.

Payri, R., Salvador, F.J., Carreres, M., Belmar-Gil, M., "Thermal effects on the diesel injector performance through adiabatic 1D modelling. Part II: Model validation, results of the simulations and discussion", Fuel 260:115663 (author version).

doi: 10.1016/j.fuel.2019.115663

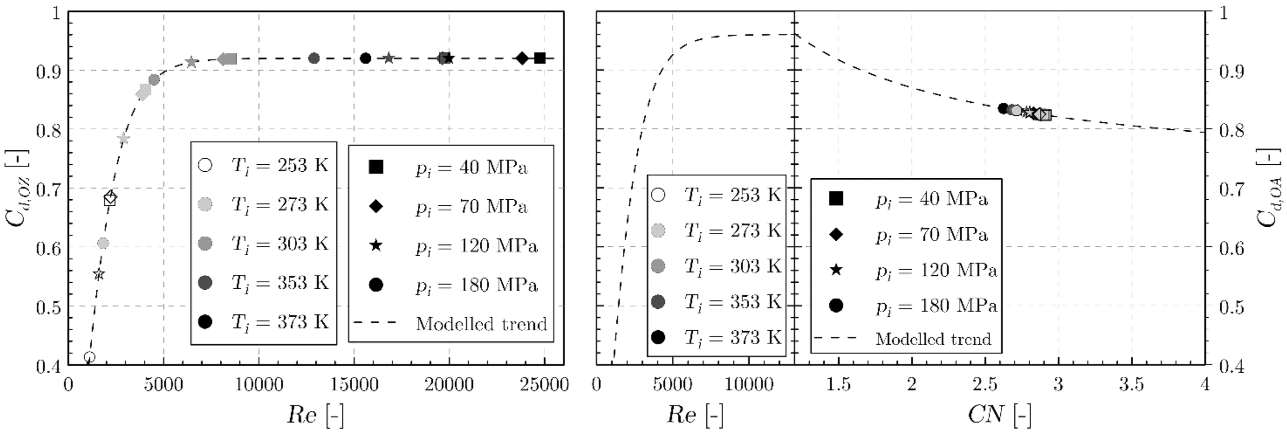

(a) OZ orifice. (b) OA orifice.

Figure 8. Discharge coefficient predicted for the control volume orifices according to the flow regime set during the opening stage at the tested operating conditions.

In the case of the OA orifice, the analogous results of temperature change across the restriction are shown in Figure **7(c)** and Figure **7(d)**. The temperature upstream of this orifice matches the one downstream of OZ (as per **Figure 7(a)** and **Figure 7(b)**). Therefore, the complete temperature variation from the injector inlet to the fuel return line is the addition of both values of ΔT. In this case, the fuel only crosses the orifice while the electromagnetic valve is open (recall **Figure 1**). During this period, the temperature change is almost constant with time. The magnitude of the temperature rise along this orifice is greater than the one reported for OZ. This is due to the larger pressure drop expected across this orifice for the injector operating conditions, since the fuel is discharged from the control volume to the return side of the injector (at atmospheric pressure) through this orifice and some minor hydraulic restrictions in the solenoid valve (depicted in the model sketch from **Figure 1**). The absolute pressure drop along this orifice is higher the larger the injection pressure, justifying the findings from **Figure 7(c)** and **Figure 7(d)** for which the temperature variation grows higher with the injection pressure. For this orifice, the values of $\Delta T_{OA,max}$ shown in **Figure 7(d)** are representative of both the opening and closing stages of the injection event. The temperature rise across this orifice is mostly governed by the injection pressure, with only a marginal influence of the fuel temperature at the injector inlet. This low influence of T_i can be attributed to the fact that the flow through OZ is prone to cavitate, as depicted in **Figure 2(b)**. **Figure 8(b)** shows the discharge coefficient predicted for OZ at the injector opening stage. The modelled trends for C_d as a function of *Re* (for non-cavitating conditions) and the so-called cavitation number *CN* (for the cavitating ones) are shown, together with the points corresponding to the variables induced for each injector operating condition. *CN* is defined by Eq. (4) (for more details on the significance of this variable, please refer to some works where it was introduced [26] and applied [17]):

$$CN = \frac{p_{up} - p_{dw}}{p_{dw} - p_v} \quad (4)$$

Figure 8(b) then shows that cavitation appears for all the injector operating conditions tested due to the large pressure drops established across OZ. This implies that C_d is not dependent on *Re* (which varies with the fuel properties induced by each condition of temperature and pressure) but rather on *CN* (which exclusively depends on the pressure ratio among upstream and downstream pressure). As it can be seen in the figure, *CN* takes similar values regardless the injection pressure tested (since the pressure drop from the control volume to the atmospheric pressure is proportionally splitted among the OA orifice and the minor restrictions in the solenoid valve shown in **Figure 1**), not significantly modifying C_d. The low differences among temperature rise observed for the different values of T_i could be attributed to these marginal differences. In addition, the temperature upstream of OA has already been submitted to the temperature change through OZ, meaning that the different temperature rises induced in OZ depending on the injection pressure and temperature also influence the starting temperature for the expansion across OA.

As far as the nozzle feeding line (NFL) is concerned, this line contains the flaps (see **Figure 1**) as a significant constraint to the flow. These restrictions impose the pressure losses responsible for the temperature variations shown in **Figure 7(e)** and **Figure 7(f)**, which need to be taken into account to determine the conditions right upstream of the nozzle orifices. In this case, the maximum temperature variations take place when the solenoid valve stops being energized. The magnitude of the temperature changes is not relevant at low injection pressures, but it is not negligible from medium values of injection pressure. No significant influence of the fuel temperature at the injector inlet is noticed for the low pressure cases, although differences among temperatures are reported for higher values of injection pressure. The reasons for this behaviour are analogous to the ones given for OZ.

3.2. Analysis for the nozzle orifices

The adiabatic flow through the nozzle implies that the stagnation enthalpy is preserved, with an important change in kinetic energy along the orifices. As established by Eq. (2), the temperature downstream of the orifices depends not only on the specific enthalpy of the fuel, but also explicitly on the pressure drop across the orifices, their discharge coefficient and the fuel density, assuming $C_a \approx 1$ since cavitation was not found in the nozzle orifices of the Bosch CRI 2.20 injector (**Figure 2(a)**). It is important to remind that Eq. (2) was derived under the assumption that no net work was done on the system or by the system. As stated in the first part of the study, this assumption may not hold during the transient stages of the injection, when the low needle lift may lead to an exchange of mechanical work with the flow established through the nozzle [23]. In a previous investigation, the authors reported that the interaction among needle and nozzle flow only seems to be relevant for needle lift values lower than 75 µm [16]. This situation is restricted to about 0.1 ms during both the opening and closing stages of the injection. In this section, quantitative results are only reported for steady conditions, once the rate of injection is nearly constant with time. This will ensure that any deviation introduced by this assumption on the fuel temperature calculations is already damped by the time steady-state conditions are reached.

In any case, it is interesting to analyse the steady-state temperature change (t_{aSOE} = 1 ms for the cases of ET = 1 ms) modelled by Eq. (2) along the nozzle orifices as a function of their C_d for the different operating conditions tested (the steady values of upstream temperature and pressure passed by the nozzle feeding line discussed in Section 3.1 are thus accounted for), as shown in Figure **9**. This analysis illustrates the possible range of values of ΔT across the nozzle orifices, also serving a qualitative estimation on the expected behaviour in the transient stages of the injection: in these stages, the needle motion when discovering or covering the orifices establishes low values of *Re* that in turn lead to low values of discharge coefficient. The figure shows that, in steady-state conditions, the fuel temperature increases across the nozzle for low values of C_d, due to the important losses associated. Indeed, there is a value of C_d for which the low losses and high flow velocities result in the fuel being subcooled rather than heated. It is important to note that, given the 1D approach followed in this work, the values of ΔT presented correspond to the fuel bulk temperature. A similar result has been reported in the literature through 3D CFD approaches by Theodorakakos et al. [32] , Strotos et al. [33] and the authors [34], showing that the fuel temperature is expected to vary in the radial direction, being heated in the wall vicinities where the friction losses are located (boundary layer) and being subcooled near the orifices axes.

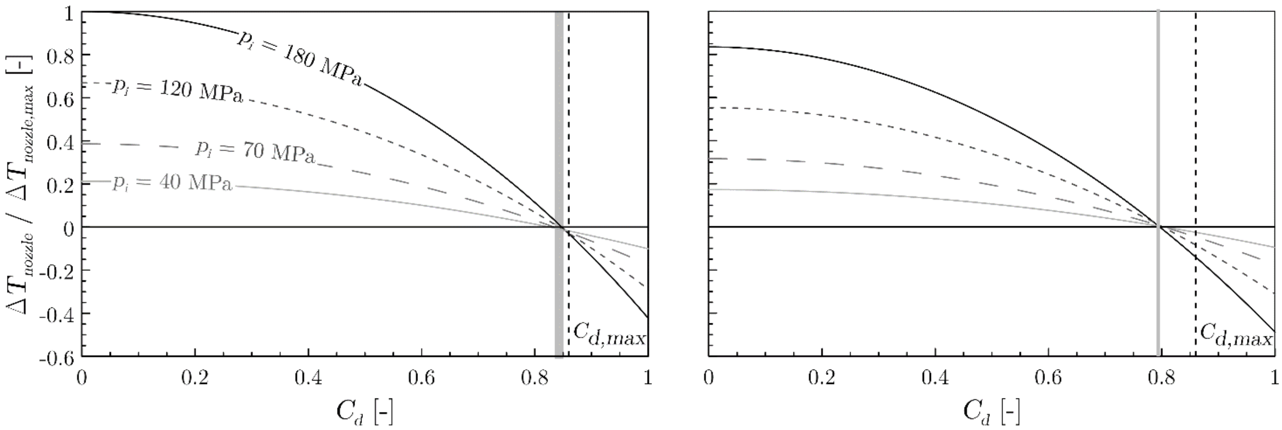

(a) $T_i = 253$ K. (b) $T_i = 373$ K.

Figure 9. Steady-state temperature change across the nozzle as a function of the discharge coefficient (t_{aSOE} = 1ms, ET = 1ms). Values normalized with $\Delta T_{nozzle,max}$ = 71.4 K (found for T_i = 253 K and p_i = 180 MPa). $C_{d,max}$ is also represented. The shaded bands highlight the transitional C_d for which the flow stops being heated and is subcooled.

The transitional *Cd* among heating and cooling in steady-state conditions is slightly lower than the maximum discharge coefficient of the nozzle orifices. Hence, situations for which the fuel cools upon expansion through the nozzle may be present. As can be seen in **Figure 9**, the fuel is expected to heat more importantly the lower T_i for low values of C_d. As it happened for the OA orifice, this can also be related to the different values of pressure and temperature set upstream of the nozzle after the losses through the NFL restriction. The effect of T_i on the temperature change through the nozzle also leads to the transitional discharge coefficient among heating and cooling being lower the higher the value of T_i. Hence, the difference among this transitional C_d and $C_{d,max}$ gets higher, leaving room for a more important cooling effect the higher T_i.

In the view of these observations, the fuel temperature is expected to increase across the nozzle during the injector opening and closing transient stages. The low needle lifts impose a restriction to the flow that results in a lower effective cross-sectional area (i.e. lower effective diameter) of the orifices, implying a lower *Re* and higher losses that in turn lead to low values of discharge coefficient. Once steady conditions are achieved, C_d is expected to become higher and the pressure drop across the nozzle reaches the conditions for which the temperature changes were displayed in **Figure 9**. The magnitude of these temperature changes then depends on the flow regime established by each operating condition. In order to analyse them, **Figure 10(a)** shows the flow regime established through the nozzle orifices in steady conditions for each operating condition tested.

- As it can be seen on the one hand, values of temperature at the injector inlet above a certain threshold (found to be $T_i \approx 283$ K) lead to the nozzle working in the turbulent regime regardless of the injection pressure, implying $C_{d,max}$ is reached. In these cases, the losses through the orifices are small, minimizing the viscous friction near the orifice walls and thus leading to the fuel being subcooled (mainly in the centre of the orifice) during the steady-state stage. The values of this cooling are reported in **Figure 10(b)**, where the justified low influence of the injection pressure is observed. The fact that a slightly greater cooling is observed for $T_i = 373$ K can be explained since the value of C_d showing the transition among the cooling and heating effects departs more importantly from $C_{d,max}$ the higher the fuel temperature, as stated in the view of **Figure 9**. In any case, the magnitude of this cooling is not high: considering the addition of the heating effect observed along the nozzle feeding line, it is possible to state that the fuel does not significantly change its temperature from the injector inlet to the nozzle outlet in steady-state conditions. Next, there will be a transitional time during the injection event (corresponding to a certain needle lift) from which the fuel stops being subcooled in order to be heated again during the closing stage.
- On the other hand, the nozzle orifices work in the laminar-turbulent transition for temperatures below a certain threshold ($T_i \approx 283$ K), even during the steady-state stage, due to the exponential increase of the fuel viscosity

Payri, R., Salvador, F.J., Carreres, M., Belmar-Gil, M., "Thermal effects on the diesel injector performance through adiabatic 1D modelling. Part II: Model validation, results of the simulations and discussion", Fuel 260:115663 (author version).

doi: 10.1016/j.fuel.2019.115663

when both high pressures and low temperatures are combined. The variations in injection pressure strongly modify the injector discharge coefficient through the Reynolds number, both by means of the effective velocity and the fuel viscosity again. In these cases (even though to a lower extent than during the transient stages) the fuel keeps being heated during the whole injection event. The values of ΔT achieved during the steady-state stage are shown in **Figure 10(b)**. This heating is more important the higher the injection pressure, displaying a non-linear trend. This can be justified in the view of Eq. (2) by the combination of pressure drop and discharge coefficient. The magnitude of this heating effect, added to the heating observed along the nozzle feeding line, may importantly influence the flow conditions downstream of the nozzle and the spray development, especially considering the high sensitivity of the fuel viscosity to changes in fuel temperature for cold conditions.

It is important to note that, if $C_{d,max}$ had been higher for the injector nozzle, a lower heating effect would have been observed for low values of T_i and a greater cooling effect would have been observed for high values of T_i. On the contrary, higher temperatures at the nozzle outlet would have been observed if $C_{d,max}$ had been lower, even leading to a net heating for high values of T_i. Also, if $C_{d,max}$ had been higher (keeping the same value of critical Re for transition among laminar and turbulent regime), those operating conditions now leading to the laminar-turbulent transition in **Figure 10** would still lead to this transitional regime. However, the slope of the curve in this transitional region would be greater, leading to a lower heating effect (or even a cooling) being observed for low values of T_i. Hence, higher values of $C_{d,max}$ imply a reduction in the threshold value for T_i below which the fuel is heated along the nozzle instead of being cooled down. Additionally, operating conditions for which steady conditions are not achieved (i.e. low ET) may result in the fuel being importantly heated at all times.

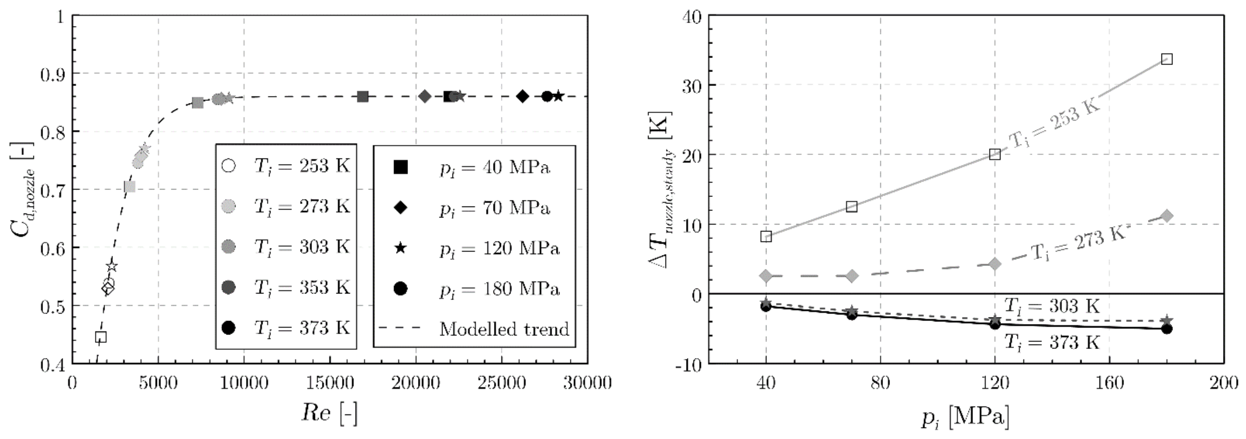

(a) Established flow regime. (b) Temperature change.

Figure 10. Predicted discharge coefficient and temperature change along the nozzle orifices according to the flow regime set during the steady-state stage at the tested operating conditions (t_{aSOE} = 1 ms for injections with ET = 1ms).

Additionally, it may be seen that the fuel temperature changes along the nozzle tend to reduce the initial differences among extreme conditions (the fuel initially colder is heated along the nozzle, whereas the fuel initially warmer is cooled along the nozzle). This acts in the sense of reducing the differences in fuel density and fuel viscosity among cases, thus contributing to the small difference in steady-state stage ROI identified in Section 2.4 in the view of the experimental results of Figure **5**.

Last, it is interesting to analyse at this point the influence of the deviations among the predicted and the measured ROI pointed out by the validation (**Figure 5**) on the estimated temperature changes across the nozzle. In this sense, the operating conditions for which the greatest differences in the ROI curves were found (low injection pressures for T_i = 253 K) lead to under-predictions in the specific enthalpy change along the orifices. This in turn leads to under-predictions in the fuel temperature changes, quantified as 5 K and 3 K, respectively. The lower deviations in ROI found in the rest of the cases would lead to negligible uncertainties in these predictions (in the order of 1 K).

4. ANALYSIS OF THE INJECTOR DYNAMICS

As the experimental ROI curves demonstrated (see Figure **5**), the operation of the Bosch CRI 2.20 injector leads to a different dynamic behaviour (namely delay among the start of energizing and start of injection, injector opening slope and injector duration) for a single injection depending on the fuel injection pressure and temperature at the injector inlet. The differences in injection duration have been attributed to the ballistic nature of the injector, since the varied operating conditions lead to different top values of needle lift from which the needle has to fall in order to close against its seat. The present section aims at the observation of the injector internal features by means of the implemented adiabatic model in order to fully understand these differences. Later on, the hydraulic performance of the injector under split injection strategies is also examined thanks to the model.

4.1. Analysis of the forces driving the needle motion

Injector dynamics is mainly driven by the forces acting on the needle, which are mainly due to two contributions:

$$F_{needle} = F_{\Delta p} - F_{fric} \tag{5}$$

where $F_{\Delta p}$ is the force due to the pressure difference among the upper part of the needle (control volume in Figure **1**) and its lower part, acting in the sense of the needle motion; whereas F_{fric} is the force generated by viscous friction in the clearance between the needle and the injector wall (especially relevant when this clearance is small), opposing the needle motion.

The term $F_{\Delta p}$ in Eq. (5) is governed by the performance of the control volume orifices analysed in Section 3.1, since the flow rate through them determines the ability to generate the pressure drop at the control volume when the solenoid valve is energized (making the needle rise, discovering the nozzle orifices) or to restore it when the injector stops being energized (making the needle close against its seat). Figure **11** shows the evolution of the pressure in the control volume (normalized with the injection pressure) responsible for this force for some of the operating conditions tested, focusing on the cases of ET = 1ms. The figure shows that, for any injection pressure condition, the depression generated in the control volume during the opening stage occurs earlier and achieves a greater magnitude the lower the fuel temperature. This result can be explained due to the different flow regime established at both control orifices depending on the injector operating conditions. As shown in Figure **8**, the range of values taken by the discharge coefficient of the OA orifice is not wide. In the case of OZ, however, important differences were seen depending on the injection operating conditions: for a given injection pressure, the discharge coefficient was lesser the lower the fuel temperature. This implies higher pressure losses through the orifice that result in an earlier and larger pressure drop, explaining the trends observed in Figure **11**. On the other hand, Figure **11** shows that it takes longer for the control volume to restore its pressure the higher the value of T_i once the injector stops being energized. At this instant, the OA orifice is locked and OZ is responsible for re-establishing the pressure in the volume. This behaviour may be justified by the mass flow rate through the orifice: even though C_d is higher for high values of T_i, the pressure drop that it induces across the orifice is lower, resulting in a lesser theoretical flow velocity. In addition, the fuel density is considerably lower when compared to the one at cold conditions. These two factors are able to overcome the effect of the discharge coefficient and lead to small mass flow rates through the orifice. As a consequence, longer times are needed for the control volume to restore the rail pressure, as observed. No significant influence of the injection pressure is noticed on the normalized pressure drops in the control volume, although a greater influence among temperatures is seen the higher the injection pressure.

Payri, R., Salvador, F.J., Carreres, M., Belmar-Gil, M., “Thermal effects on the diesel injector performance through adiabatic 1D modelling. Part II: Model validation, results of the simulations and discussion”, Fuel 260:115663 (author version).

doi: 10.1016/j.fuel.2019.115663

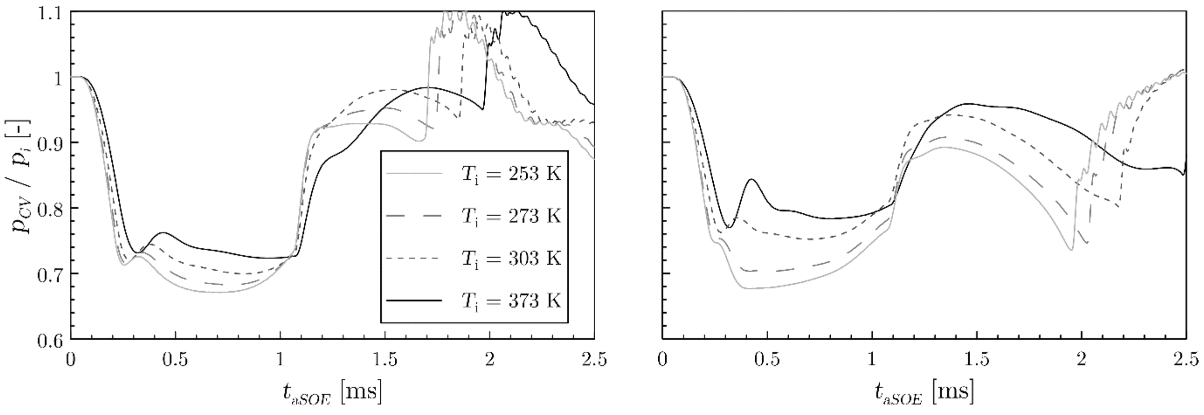

(a) $p_i = 40$ MPa. (b) $p_i = 180$ MPa.

Figure 11. Temporal evolution of the pressure in the control volume (normalized with the injection pressure) for some operating conditions tested (ET = 1ms).

It is important to note that the sole effect of the discussed hydraulic parameters of the control volume orifices would lead to a faster response of the injector at low temperatures, since the more accused pressure drop at the control volume would generate a higher unbalance at both sides of the needle.

The second term of Eq. (5), F_{fric}, is modelled according to Eq. (6) [35]:

$$F_{fric} = F_{fric,\mu} - F_{fric,\Delta p} = 4\pi\mu_f U_n L_{cl}\left(\frac{D_{pist}}{D_{cl}} - 1\right) - \pi\frac{D_{cl}}{2}\frac{D_{pist} - D_{cl}}{2}\Delta p_{cl} \qquad (6)$$

As it may be seen, the friction force appearing on the needle depends both on the fuel viscosity (which in turn depends on fuel temperature and pressure) and the pressure losses along the part of the needle where the clearance is small (Δp_{cl}, concentrated in the upper part of the needle –right below the control volume- as seen in Figure **1**), with opposed effects. It is then interesting to determine which of the two terms in Eq. (6) plays a more significant role in the needle motion of the diesel injector. Figure **12** shows the value of the ratio among $F_{fric,\mu}$ and $F_{fric,\Delta p}$ along part of an injection event for some of the tested conditions. The figure only shows the time range corresponding to the stage in which the needle is rising. As it may be seen, the term related to fuel viscosity is several orders of magnitude higher than the one related to the pressure drop. In addition, its influence is even more important the lower the fuel temperature at the injector inlet and the higher the injection pressure, due to the high viscosities associated. Hence, it is possible to state that the net effect of increasing the fuel temperature is a reduction in the friction force, which would in turn act in the sense of a faster needle opening.

Payri, R., Salvador, F.J., Carreres, M., Belmar-Gil, M., "Thermal effects on the diesel injector performance through adiabatic 1D modelling. Part II: Model validation, results of the simulations and discussion", Fuel 260:115663 (author version).

doi: 10.1016/j.fuel.2019.115663

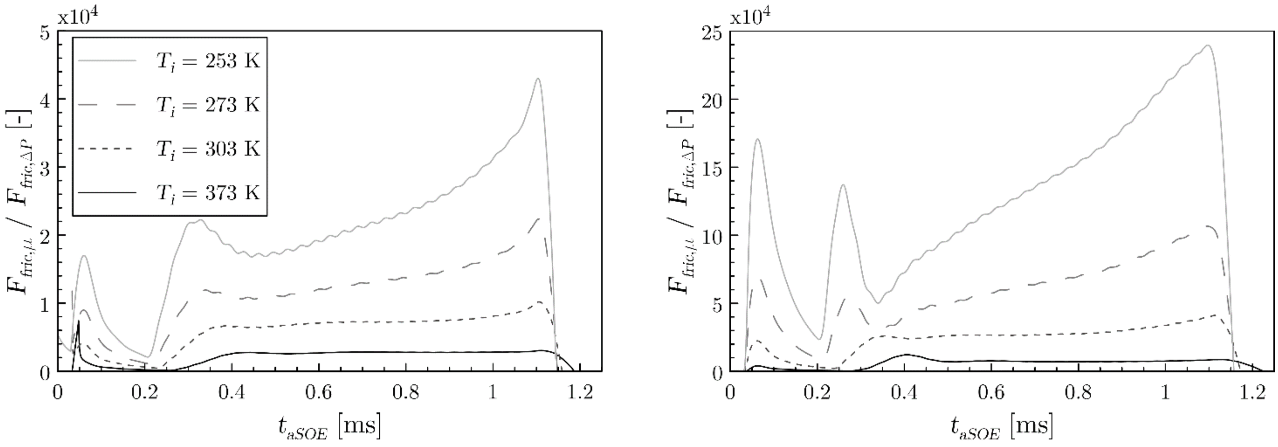

(a) $p_i = 40$ MPa. (b) $p_i = 180$ MPa.

Figure 12. Temporal evolution of the ratio among the viscous force on the needle generated by fuel viscosity and the one induced by the pressure losses along the part of the needle with a small clearance (ET = 1 ms).

From the previous considerations, it follows that there are two opposed effects of the fuel temperature on injector dynamics: a lower fuel temperature would lead to a faster injector opening if only the pressure forces were considered, whereas it would lead to a slower opening by the sole effect of viscous friction. These opposed effects of the fuel temperature on injector dynamics have already been found in previous works by the authors [36,37] and reported in the literature [21]. In order to observe how they are translated into needle motion, Figure **13** shows the evolution of the needle lift computed by the model. The figure shows that the time at which the injector closes depends on the fuel temperature at the injector inlet, as was observed experimentally (Figure **5**). For each injection pressure, it is observed that the needle starts to rise earlier the lower the fuel temperature. In the absence of needle motion (thus, in the absence of friction forces acting on the needle), this fact is in agreement with the findings from Figure **11** about the pressure in the control volume dropping faster and to a larger extent the lower the fuel temperature. Nevertheless, the slopes of the curves reveal that the injector opening is slower the lower the fuel temperature. This result is also aligned with the previous findings: once the needle moves, friction forces proportional to the fuel viscosity appear, opposing this motion. Given the significant increase in fuel viscosity at low temperatures (and especially at high injection pressures, for which Figure **13** shows the higher differences in opening slope), this soon results in the needle moving slower for cold conditions. Indeed, it can be seen that once the needle reaches among 5 to 10% of its maximum lift ($t_{aSOE} \approx 0.4$ ms), it has already reached upper positions the higher the fuel temperature at the injector inlet. On the other hand, as expected, the effect of the injection pressure on the opening stage is to achieve faster rates. This is explained considering the larger absolute pressure drops achieved in the control volume (Figure **11**), which generate a higher pressure unbalance among the lower and the upper side of the needle.

Payri, R., Salvador, F.J., Carreres, M., Belmar-Gil, M., "Thermal effects on the diesel injector performance through adiabatic 1D modelling. Part II: Model validation, results of the simulations and discussion", Fuel 260:115663 (author version).

doi: 10.1016/j.fuel.2019.115663

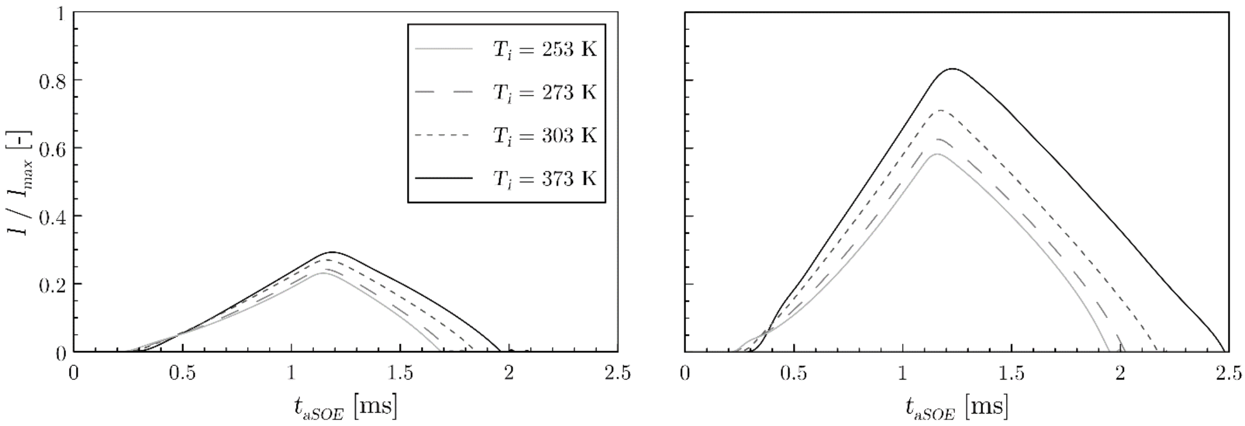

(a) $p_i = 40$ MPa. (b) $p_i = 180$ MPa.

Figure 13. Temporal evolution of the needle lift (normalized with the mechanical limit of the injector l_{max} = 850 µm) for some operating conditions tested (ET = 1 ms).

It is also confirmed that a slower needle opening results in lower top positions reached by the needle during an injection event. Hence, during the closing stage, the needle falls from lower positions the lower T_i, resulting in shorter times needed for the needle to close against its seat and cut the injection. This confirms the injection duration trends pointed out in Figure **5**. Also, the time at which the top position is reached by the needle varies depending on T_i, being achieved later the higher T_i. This finding may be justified in the view of Figure **11**, where it was observed that the pressure in the control volume was restored in a slower manner the higher T_i. This reasoning could also be valid to explain the slightly slower closing found for high values of T_i: once the needle lifts, it reduces the fuel volume at the upper part of the needle. When the needle falls back towards its seat, this volume is increased again. Therefore, it needs to be replenished with fuel in order to restore the pressure. For high values of T_i, the taller top positions reached by the needle result in a higher volume needing to be replenished during the closing in order to restore the initial pressure. However, these high values of T_i result in lower fuel densities that reduce the mass flow rate employed to that end.

In any case, an acceleration in the needle closing is observed at the end of the injection for most conditions. This acceleration, especially relevant at cold conditions, has also been reported in the literature. Moon et al. [38] observed this increase in needle speed through an X-ray imaging technique, and relate it to the sudden decrease of sac pressure due to the flow restriction (throttling) from the needle at low needle lifts. The higher restriction (i.e. lower effective discharge coefficient) generates a higher pressure drop through the needle seat. Consequently, the sac pressure decreases, generating an even higher unbalance among the pressure forces at the upper and lower sides of the needle, abruptly increasing the needle speed. Wang et al. [22] also noticed through ROI measurements that this phenomenon was especially important for cold fuel temperature conditions. They reasoned that the major friction induced by high viscosity could curb the fuel

doi: 10.1016/j.fuel.2019.115663

flow generating an even higher pressure drop in the sac.

4.2. Behaviour under multiple injections

The impact of the operating conditions on the hydraulic performance of the Bosch CRI 2.20 injector under split injection strategies has been examined by means of the implemented computational model. In order to analyse this influence, several electric dwell times (DT) among injections have been tested. DT is defined in Figure **14** as the temporal separation among the end of the energizing pulse of an injection and the beginning of the pulse of the subsequent injection.

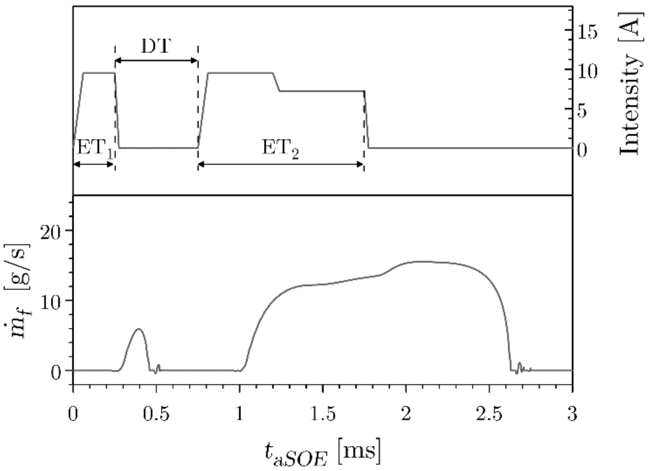

Figure 14. Definition of the electric dwell time (DT).

The time needed for the injector to stop delivering fuel once the energizing signal has ended cannot be neglected. Hence, if DT is too small, an overlapping among two subsequent injections may take place, preventing them from being splitted. A sample of this statement is shown in Figure **15** for several tested conditions including pilot plus main injection strategies and main plus post injection strategies. An important influence of the dwell time on the amount of fuel delivered by the second injection (more accused for the main plus post injection case) is observed. The pressure wave induced by the opening of the injector for the first injection is responsible for this phenomenon. As seen in Figure **4**, the pressure at the injector inlet still oscillates once the injector is effectively closed. Similarly, the pressure upstream of the nozzle orifices represented in Figure **15(c)** and Figure **15(d)** takes some time to be stabilized after a given injection. Hence, if the injector is reenergized during this period, the new injection will introduce a higher or lower amount of fuel mass than its single injection equivalent depending on the instantaneous value of pressure at the nozzle inlet. Pressure wave propagation is influenced by the fuel speed of sound and bulk modulus [19], meaning that both the amplitude and period of the pressure oscillations at the nozzle inlet will depend on fuel temperature and pressure. Thus, the injector operating conditions are expected to affect the critical dwell time to effectively separate injections and the total mass injected by the second injection.

Payri, R., Salvador, F.J., Carreres, M., Belmar-Gil, M., “Thermal effects on the diesel injector performance through adiabatic 1D modelling. Part II: Model validation, results of the simulations and discussion”, Fuel 260:115663 (author version).

doi: 10.1016/j.fuel.2019.115663

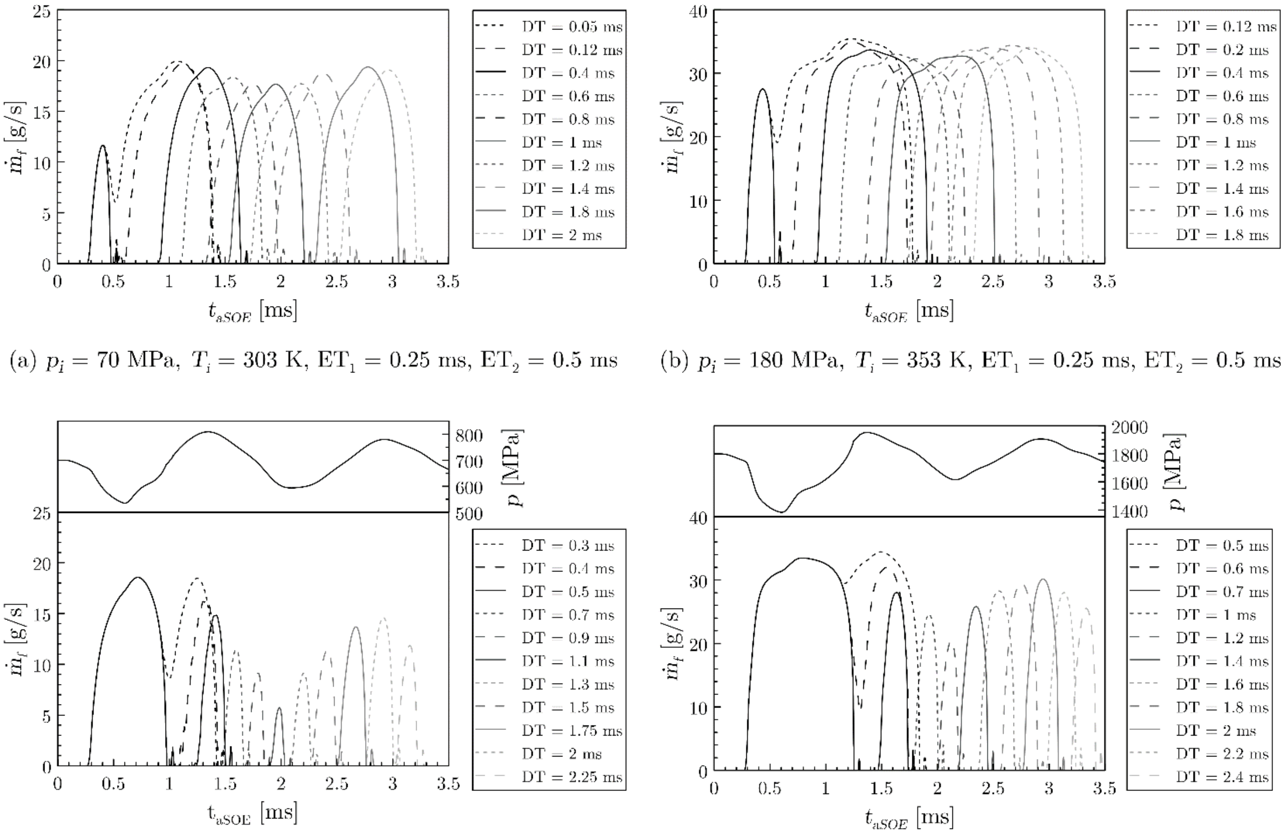

(a) $p_i = 70$ MPa, $T_i = 303$ K, $\mathrm{ET}_1 = 0.25$ ms, $\mathrm{ET}_2 = 0.5$ ms
(b) $p_i = 180$ MPa, $T_i = 353$ K, $\mathrm{ET}_1 = 0.25$ ms, $\mathrm{ET}_2 = 0.5$ ms
(c) $p_i = 70$ MPa, $T_i = 303$ K, $\mathrm{ET}_1 = 0.5$ ms, $\mathrm{ET}_2 = 0.25$ ms
(d) $p_i = 180$ MPa, $T_i = 353$ K, $\mathrm{ET}_1 = 0.5$ ms, $\mathrm{ET}_2 = 0.25$ ms

Figure 15. Modelled injection rate for pilot plus main injection strategies (a,b) and for main plus post injection strategies (c,d) for sample operating conditions. The evolution of the pressure upstream of the nozzle orifices corresponding to the single injection case equivalent to the main injection is also represented for the main plus post injection strategies.

Figure **16** shows the critical dwell time at which two desired injections stop being overlapped to be effectively separated for each of the tested values of fuel temperature at the injector inlet and injection pressure. As it may be seen in Figure **16(a)** for the pilot plus main injection strategy, the injector may be reenergized shortly after the first pulse is finished. In general, a larger separation among energizing pulses is required the higher the injection pressure and the higher T_i. This result is consistent with the trends in injection duration found experimentally (Figure **5**) and justified in Section 4.1. With regard to the main plus post injection strategy depicted in Figure **16(b)**, the same trends are observed, since the factors influencing the process remain the same. Comparatively higher values of DT_{crit} are exhibited, since the duration of the first injection directly establishes the critical dwell time to separate the next one. This reasoning remains true unless the mechanical limit of the needle is reached during the main injection, thus influencing the observed trends among operating conditions and injection duration.

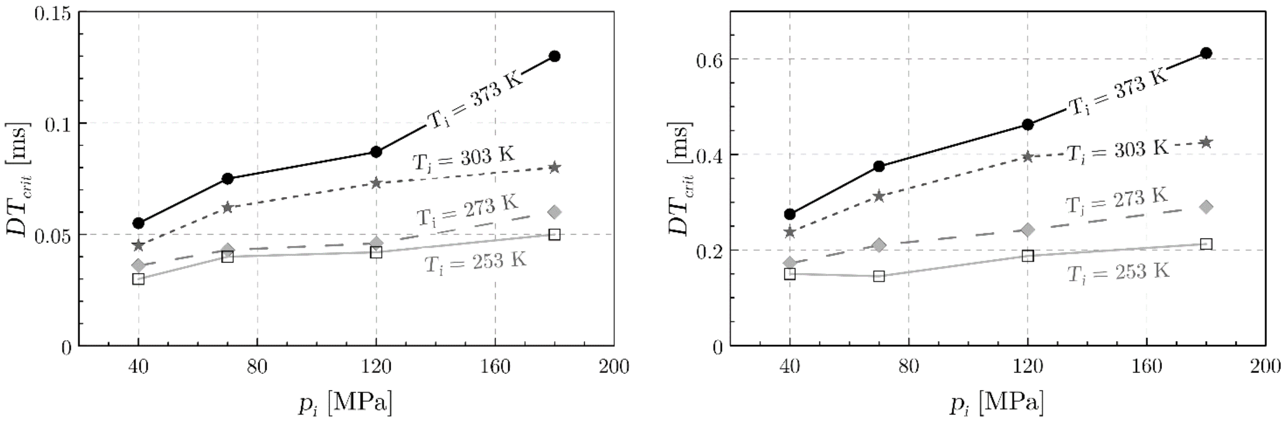

(a) Pilot plus main injection strategy. (b) Main plus post injection strategy.

Figure 16. Critical dwell time to split successive injections depending on the operating conditions (ET_{pilot} = 0.25 ms, ET_{main} = 0.5 ms, ET_{post} = 0.25 ms).

The effect of the first injection on the mass injected by the second injection has been quantified for different values of DT (higher than the critical one) for each tested condition, as shown in Figure **17**. A strong influence of the dwell time is observed in all cases. Focusing on the results found for the pilot plus main injection depicted in Figure **17(a)** and Figure **17(b)**, it may be seen that the mass values are greatly influenced for short dwell times, close to DTcrit. This leads to masses of the main injection that can even increase those of the equivalent injection by a 40%. This result, already observed by the authors [37,39], is attributed to the pressure overshoot that takes place right upstream of the nozzle orifices as observed in Figure **15(c)** and Figure **15(d)**. After a certain value of DT, this influence gets lower, obtaining masses that oscillate from about 80% to 115% of the values corresponding to the single injection. The oscillations depending on DT are also induced by the fluctuation of the pressure upstream of the nozzle, as already stated. As far as the main plus post injection strategy is concerned, as shown in Figure **17(c)** and Figure **17(d)**, the relative influence of the interaction among injections is higher, since the pressure above the nozzle is disturbed to a larger extent the longer the first injection. Masses almost 400% higher than the analogous ones for single injections may be delivered by the post injection, whereas the variability of the mass delivered depending on DT after this initial peak ranges from 10% to 200%.

Payri, R., Salvador, F.J., Carreres, M., Belmar-Gil, M., "Thermal effects on the diesel injector performance through adiabatic 1D modelling. Part II: Model validation, results of the simulations and discussion", Fuel 260:115663 (author version).

doi: 10.1016/j.fuel.2019.115663

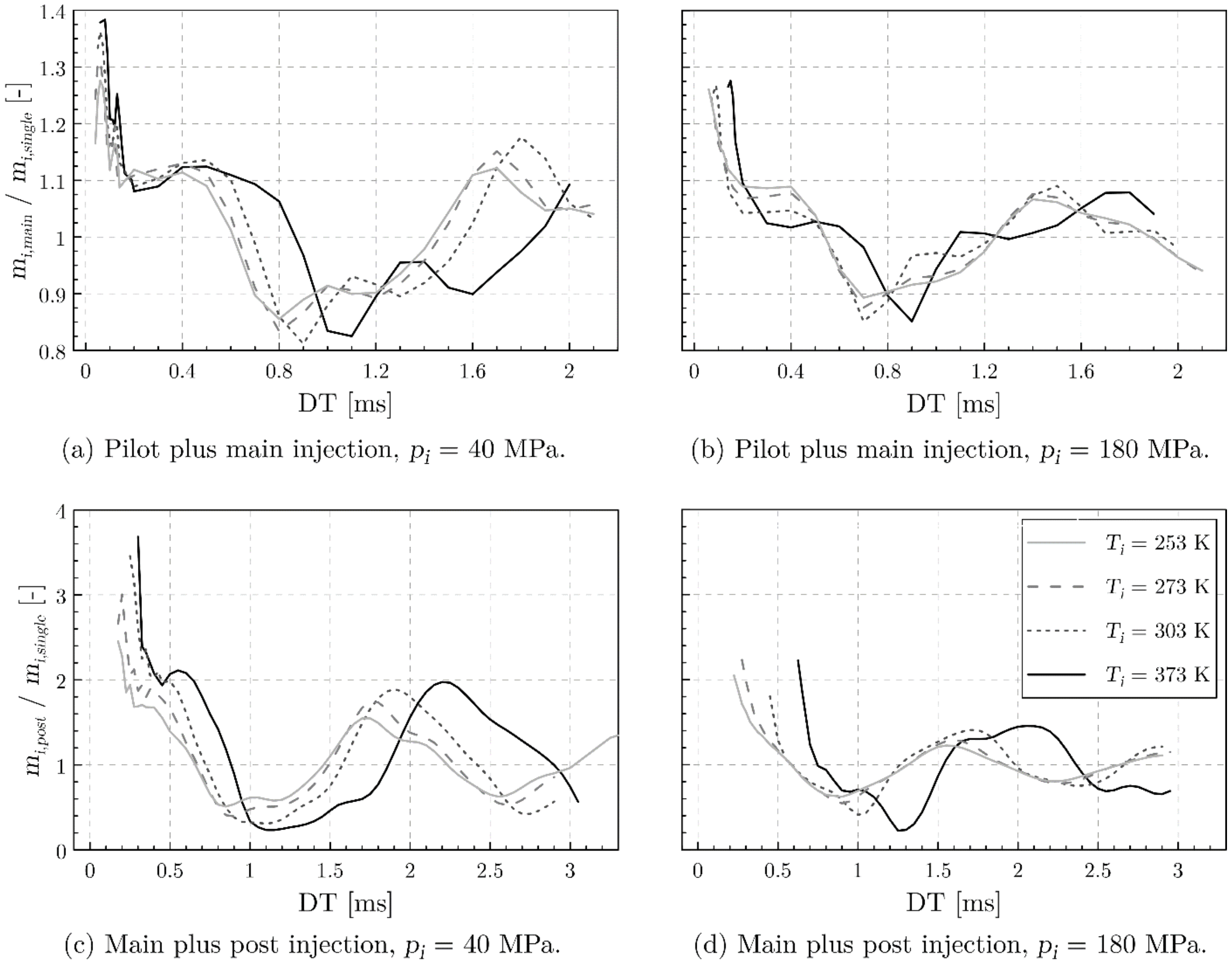

(a) Pilot plus main injection, p_i = 40 MPa.
(b) Pilot plus main injection, p_i = 180 MPa.
(c) Main plus post injection, p_i = 40 MPa.
(d) Main plus post injection, p_i = 180 MPa.

Figure 17. Fuel mass injected during the second injection for several operating conditions tested (ET_{pilot} = 0.25 ms, ET_{main} = 0.5 ms, ET_{post} = 0.25 ms). In each case, the values are normalized with the mass injected by a single injection equivalent to the second injection.

A strong influence of the fuel temperature at the injector inlet is observed on the phasing of the oscillations depending on DT. In general, the decrease of the normalised mass with DT takes place at earlier dwell times for the lowest values of T_i. This may be attributed to the higher values of fuel speed of sound and bulk modulus achieved at these temperatures [19], which reduce the period of the pressure fluctuations upstream of the nozzle once the injector is closed. The injection pressure does not seem to have such an important influence on the results. On the other hand, the variability of the mass delivered depending on DT seems to be damped the higher the injection pressure and the lower T_i. This influence of the fuel temperature on the variability of mass injected by a second injection was already reported by Wang et al. [22], who attributed it to the addition of the effects of shorter injection duration and longer injection delay induced by low temperatures.

doi: 10.1016/j.fuel.2019.115663

5. CONCLUSIONS

A computational 1D model has been used to evaluate the influence of the fuel temperature and its variations within a solenoid-driven common-rail ballistic injector on the injector performance. The model makes use of the adiabatic flow hypothesis, whose validity is assessed in the first part of the study. The model itself has been extensively validated against experimental results for a wide range of operating conditions, including several injection pressures and values of fuel temperature at the injector inlet ranging from those representative of cold start to those representative of long engine runs. The main conclusions of the use of this model are summarized as follows:

- The introduction of the adiabatic flow hypothesis allowed to extend the range of operating conditions for which the computational model is reliable, including low fuel temperatures at the injector inlet representative of cold-start.
- The fuel warms upon expansion across the control volume orifices (OZ and OA) and the nozzle feeding line during the whole injection event. These temperature increases are more relevant the higher the injection pressure, due to the larger absolute pressure drops established. In the case of the OZ orifice and the nozzle feeding line, the magnitude of the temperature increase is greater for low values of the fuel temperature at the injector inlet, since the high fuel viscosities associated to these temperatures imply low values of *Re* that induce a laminar or transitional flow regime identified with a greater heating. In the case of the OA orifice, the fuel temperature at the injector inlet does not importantly affect the temperature rise across the orifice for a given pressure, since all the operating conditions induce the same cavitating regime in the orifice.
- As far as the nozzle orifices are concerned, it may be stated that the fuel heats along the nozzle during the transient stages of the process, whereas it may be heated or subcooled during the steady-state stage depending on the discharge coefficient achieved (i.e. flow regime) and the maximum discharge coefficient of the nozzle. The magnitude of this heating or cooling is more accused the larger the injection pressure. For the particular injector studied, a threshold value of fuel temperature at the injector inlet of 283 K has been found. Above this value, the fuel is subcooled during the steady-state stage of the injection. Nevertheless, this cooling is not especially relevant (≈ 10 K) and is compensated with the heating taking place along the nozzle feeding line, allowing to state that the fuel temperature is virtually unchanged from the injector inlet to the outlet. However, fuel temperatures at the injector inlet below 283 K induce a laminar or transitional flow regime leading to an important heating. The magnitude of this heating effect, added to the one along the nozzle feeding line, may importantly influence the flow conditions downstream of the nozzle and the spray development.

Payri, R., Salvador, F.J., Carreres, M., Belmar-Gil, M., “Thermal effects on the diesel injector performance through adiabatic 1D modelling. Part II: Model validation, results of the simulations and discussion”, Fuel 260:115663 (author version).

doi: 10.1016/j.fuel.2019.115663

- Needle dynamics is influenced by the pressure unbalance established among its upper and its lower side once the injector is energized. For a given injection pressure, the depression generated in the control volume during the opening stage occurs earlier and achieves a greater magnitude the lower the fuel temperature, since the laminar or the transitional regime are established across OZ. This generates higher pressure losses across the orifice, further reducing the pressure in the control volume and influencing the delay among the start of energizing and the start of injection. Once the needle starts moving, its lifting velocity not only depends on the pressure unbalance at both sides of the needle, but also on the viscous friction opposing the needle motion. This effect is more important the lower the fuel temperature, due to the important increase in viscosity. As a result, once the solenoid stops being energized, the needle will fall from different positions depending on the operating condition, taking more or less time to close against its seat and influencing the injection duration.
- In terms of split injection strategies, fuel properties influence the critical dwell time that allows to totally separate two subsequent injections. In general, this time is higher the higher the fuel temperature and the injection pressure, since the needle falls from an upper position in these conditions. The timing among injections affects the total mass injected by the second injection differently depending on the injection pressure and the fuel temperature at the injector inlet, due to the different induced values of speed of sound and bulk modulus affecting pressure wave propagation. In addition, the variability in fuel mass injected depending on the dwell time is more accused the higher the fuel temperature.

ACKNOWLEDGEMENTS

This work was partly sponsored by FEDER and the Spanish “Ministerio de Economía y Competitividad” in the frame of the project “Desarrollo de modelos de combustión y emisiones HPC para el análisis de plantas propulsivas de transporte sostenible (CHEST)”, reference TRA2017-89139-C2-1-R-AR. On the other hand, the support given to Mr Mario Belmar by “Universitat Politècnica de València” through the “FPI-Subprograma 2” grant within the “Programa de Apoyo para la Investigación y Desarrollo (PAID-01-18)” is gratefully acknowledged by the authors.

The authors would also like to thank Mariano Sánchez for his technical help.

REFERENCES

[1] Lefèbvre AH. Atomization and Sprays. CRC Press; 1988.

[2] Gumus M, Sayin C, Canakci M. The impact of fuel injection pressure on the exhaust emissions of a direct

injection diesel engine fueled with biodiesel-diesel fuel blends. Fuel 2012;95:486–94. doi:10.1016/j.fuel.2011.11.020.

[3] Agarwal AK, Dhar A, Gupta JG, Kim W Il, Choi K, Lee CS, et al. Effect of fuel injection pressure and injection timing of Karanja biodiesel blends on fuel spray, engine performance, emissions and combustion characteristics. Energy Convers Manag 2015;91:302–14. doi:10.1016/j.enconman.2014.12.004.

[4] Zecca A, Chiari L. Fossil-fuel constraints on global warming. Energy Policy 2010;38:1–3. doi:10.1016/j.enpol.2009.06.068.

[5] Wang J, Feng L, Tang X, Bentley Y, Höök M. The implications of fossil fuel supply constraints on climate change projections: A supply-side analysis. Futures 2017;86:58–72. doi:10.1016/j.futures.2016.04.007.

[6] Wang X, Huang Z, Zhang W, Abiola O, Nishida K. Effects of ultra-high injection pressure and micro-hole nozzle on flame structure and soot formation of impinging diesel spray. Appl Energy 2011;88:1620–8. doi:10.1016/j.apenergy.2010.11.035.

[7] Boccardo G, Millo F, Piano A, Arnone L, Manelli S, Fagg S, et al. Experimental investigation on a 3000 bar fuel injection system for a SCR-free non-road diesel engine. Fuel 2019;243:342–51. doi:10.1016/j.fuel.2019.01.122.

[8] Mancaruso E, Sequino L, Vaglieco BM. Analysis of the pilot injection running Common Rail strategies in a research diesel engine by means of infrared diagnostics and 1d model. Fuel 2016;178:188–201. doi:10.1016/j.fuel.2016.03.066.

[9] Breda S, D'Orrico F, Berni F, D'Adamo A, Fontanesi S, Irimescu A, et al. Experimental and numerical study on the adoption of split injection strategies to improve air-butanol mixture formation in a DISI optical engine. Fuel 2019;243:104–24. doi:10.1016/j.fuel.2019.01.111.

[10] Wang B, Pamminger M, Vojtech R, Wallner T. Impact of injection strategies on combustion characteristics, efficiency and emissions of gasoline compression ignition operation in a heavy-duty multi-cylinder engine. Int J Engine Res 2018:146808741880166. doi:10.1177/1468087418801660.

[11] Desantes JM, García-Oliver JM, García A, Xuan T. Optical study on characteristics of non-reacting and reacting diesel spray with different strategies of split injection. Int J Engine Res 2018. doi:10.1177/1468087418773012.

[12] Sun Z-Y, Li G-X, Chen C, Yu Y-S, Gao G-X. Numerical investigation on effects of nozzle's geometric parameters on the flow and the cavitation characteristics within injector's nozzle for a high-pressure common-

Payri, R., Salvador, F.J., Carreres, M., Belmar-Gil, M., "Thermal effects on the diesel injector performance through adiabatic 1D modelling. Part II: Model validation, results of the simulations and discussion", Fuel 260:115663 (author version).

doi: 10.1016/j.fuel.2019.115663

rail DI diesel engine. Energy Convers Manag 2015;89:843–61. doi:10.1016/j.enconman.2014.10.047.

[13] Torelli R, Som S, Pei Y, Zhang Y, Traver M. Influence of fuel properties on internal nozzle flow development in a multi-hole diesel injector. Fuel 2017;204:171–84. doi:10.1016/j.fuel.2017.04.123.

[14] Salvador FJ, De la Morena J, Crialesi-Esposito M, Martínez-López J. Comparative study of the internal flow in diesel injection nozzles at cavitating conditions at different needle lifts with steady and transient simulations approaches. Proc Inst Mech Eng Part D J Automob Eng 2018;232:1060–78. doi:10.1177/0954407017725672.

[15] Ihme M, Ma PC, Bravo L. Large eddy simulations of diesel-fuel injection and auto-ignition at transcritical conditions. Int J Engine Res 2019;20:58–68. doi:10.1177/1468087418819546.

[16] Desantes JM, Salvador FJ, Carreres M, Martínez-López J. Large-eddy simulation analysis of the influence of the needle lift on the cavitation in diesel injector nozzles. Proc Inst Mech Eng Part D J Automob Eng 2014;229:407–23. doi:10.1177/0954407014542627.

[17] Payri R, Salvador FJ, Carreres M, De la Morena J. Fuel temperature influence on the performance of a last generation common-rail diesel ballistic injector. Part II: 1D model development, validation and analysis. Energy Convers Manag 2016;114:376–91. doi:10.1016/j.enconman.2016.02.043.

[18] Salvador FJ, Carreres M, Crialesi-Esposito M, Plazas AH. Determination of critical operating and geometrical parameters in diesel injectors through one dimensional modelling, design of experiments and an analysis of variance. Proc Inst Mech Eng Part D J Automob Eng 2018;232:1762–81. doi:10.1177/0954407017735262.

[19] Desantes JM, Salvador FJ, Carreres M, Jaramillo D. Experimental Characterization of the Thermodynamic Properties of Diesel Fuels Over a Wide Range of Pressures and Temperatures. SAE Int J Fuels Lubr 2015;8:2015-01–0951. doi:10.4271/2015-01-0951.

[20] Dernotte J, Hespel C, Houille S, Foucher F, Mounaïm-Rousselle C. Influence of Fuel Properties on the Diesel Injection Process in Nonvaporizing Conditions. At Sprays 2012;22:461–92. doi:10.1615/AtomizSpr.2012004401.

[21] Park Y, Hwang J, Bae C, Kim K, Lee J, Pyo S. Effects of diesel fuel temperature on fuel flow and spray characteristics. Fuel 2015;162:1–7. doi:10.1016/j.fuel.2015.09.008.

[22] Wang Z, Ding H, Wyszynski ML, Tian J, Xu H. Experimental study on diesel fuel injection characteristics under cold start conditions with single and split injection strategies. Fuel Process Technol 2015;131:213–22. doi:10.1016/j.fuproc.2014.10.003.

[23] Salvador FJ, Gimeno J, Martín J, Carreres M. Thermal effects on the diesel injector performance through

Payri, R., Salvador, F.J., Carreres, M., Belmar-Gil, M., "Thermal effects on the diesel injector performance through adiabatic 1D modelling. Part II: Model validation, results of the simulations and discussion", Fuel 260:115663 (author version).

doi: 10.1016/j.fuel.2019.115663

adiabatic 1D modelling. Part I: Model description and assessment of the adiabatic flow hypothesis. Fuel 2019;In review.

[24] Salvador FJ, Gimeno J, Carreres M, Crialesi-Esposito M. Experimental assessment of the fuel heating and the validity of the assumption of adiabatic flow through the internal orifices of a diesel injector. Fuel 2017;188:442–51. doi:10.1016/j.fuel.2016.10.061.

[25] Nurick WH. Orifice cavitation and its effects on spray mixing. J Fluids Eng 1976;98:681–7.

[26] Soteriou C, Andrews R, Smith M. Direct Injection Diesel Sprays and the Effect of Cavitation and Hydraulic Flip on Atomization. SAE Pap 950080 1995. doi:10.4271/950080.

[27] Lichtarowicz AK, Duggins RK, Markland E. Discharge coefficients for incompressible non-cavitating flow through long orifices. J Mech Eng Sci 1965;7:210–9. doi:10.1243/JMES_JOUR_1965_007_029_02.

[28] Franc J-P. The Rayleigh-Plesset equation: a simple and powerful tool to understand various aspects of cavitation. Fluid Dyn. Cavitation Cavitating Turbopumps, vol. 496, Vienna: Springer; 2007, p. 1–41. doi:10.1007/978-3-211-76669-9_1.

[29] Payri R, Garcia-Oliver JM, Salvador FJ, Gimeno J. Using spray momentum flux measurements to understand the influence of diesel nozzle geometry on spray characteristics. Fuel 2005;84:551–61. doi:10.1016/j.fuel.2004.10.009.

[30] Salvador FJ, Gimeno J, Carreres M, Crialesi-Esposito M. Fuel temperature influence on the performance of a last generation common-rail diesel ballistic injector. Part I: Experimental mass flow rate measurements and discussion. Energy Convers Manag 2016;114:364–75. doi:10.1016/j.enconman.2016.02.042.

[31] Payri R, Salvador FJ, Gimeno J, Bracho G. A new methodology for correcting the signal cumulative phenomenon on injection rate measurements. Exp Tech 2008;32:46–9. doi:10.1111/j.1747-1567.2007.00188.x.

[32] Theodorakakos A, Strotos G, Mitroglou N, Atkin C, Gavaises M. Friction-induced heating in nozzle hole micro-channels under extreme fuel pressurisation. Fuel 2014;123:143–50. doi:10.1016/j.fuel.2014.01.050.

[33] Strotos G, Koukouvinis P, Theodorakakos A, Gavaises M, Bergeles G. Transient heating effects in high pressure Diesel injector nozzles. Int J Heat Fluid Flow 2015;51:257–67. doi:10.1016/j.ijheatfluidflow.2014.10.010.

[34] Salvador FJ, Carreres M, De la Morena J, Martínez-Miracle E. Computational assessment of temperature variations through calibrated orifices subjected to high pressure drops: Application to diesel injection nozzles. Energy Convers Manag 2018;171:438–51. doi:10.1016/j.enconman.2018.05.102.

doi: 10.1016/j.fuel.2019.115663

[35] Blackburn J, Reethof G, Shearer J. Fluid Power Control. Cambridge MA: The MIT Press; 1960.

[36] Payri R, Salvador FJ, Gimeno J, Bracho G. Effect of fuel properties on diesel spray development in extreme cold conditions. Proc Inst Mech Eng Part D, J Automob Eng 2008;222:1743–53. doi:10.1243/09544070JAUTO844.

[37] Salvador FJ, Gimeno J, De la Morena J, Carreres M. Using one-dimensional modeling to analyze the influence of the use of biodiesels on the dynamic behavior of solenoid-operated injectors in common rail systems: Results of the simulations and discussion. Energy Convers Manag 2012;54:122–32. doi:10.1016/j.enconman.2011.10.007.

[38] Moon S, Gao Y, Park S, Wang J, Kurimoto N, Nishijima Y. Effect of the number and position of nozzle holes on in- and near-nozzle dynamic characteristics of diesel injection. Fuel 2015;150:112–22. doi:10.1016/j.fuel.2015.01.097.

[39] Payri R, De la Morena J, Pagano V, Hussain A, Sammut G, Smith L. One-dimensional modeling of the interaction between close-coupled injection events for a ballistic solenoid injector. Int J Engine Res 2018. doi:10.1177/1468087418760973.

Payri, R., Salvador, F.J., Carreres, M., Belmar-Gil, M., “Thermal effects on the diesel injector performance through adiabatic 1D modelling. Part II: Model validation, results of the simulations and discussion”, Fuel 260:115663 (author version).

doi: 10.1016/j.fuel.2019.115663